Option-Implied Intra-Horizon Risk and First-Passage Disentanglement*

Markus Leippold† Nikola Vasiljević‡

June 29, 2016

Abstract

We study the intra-horizon value at risk (iVaR) in a general jump diffusion setup and propose a new model of asset returns called displaced mixed-exponential model, which can arbitrarily closely approximate finite-activity jump-diffusions and completely monotone Levy processes. We derive analytical results for the iVaR and disentangle the risk contribution of jumps from diffusion. Estimating the iVaR for several popular jump models using on S&P 100 option data, we find that option-implied estimates are much more responsive to market changes relative to their historical counterparts. Moreover, disentangling jumps from diffusion, jump account for about 90 percent of iVaR on average.

Keywords: value at risk, intra-horizon risk, displaced mixed-exponential model, first-passage disentanglement, option-implied estimates.

JEL classification: G01, G11, G13, C51, C52.

*We thank Carol Alexander, Miloš Božović, Jérôme Detemple, Walter Farkas, Fulvia Fringuellotti, Sergey Gelman, Loriano Mancini, Milan Nedeljković, Jakub Rojček, Rasmus Rousing, Davide Tedeschini, Adriano Tosi, Branko Urošević and the participants at the Brown Bag Lunch Seminar at the Department of Banking and Finance Institute at the University of Zürich, the Gerzensee Research Days 2015, and the Belgrade Young Economists Conference 2016 for their valuable comments and suggestions. We gratefully acknowledge financial support from the Swiss Finance Institute (SFI) and Bank Vontobel.

†University of Zurich and Swiss Finance Institute, Plattenstrasse 14, 8032 Zurich, Switzerland; e-mail: markus.leippold@bf.uzh.ch.

‡Corresponding author. University of Zurich and Swiss Finance Institute, Plattenstrasse 14, 8032 Zurich, Switzerland; e-mail: nikola.vasiljevic@bf.uzh.ch.

1 Introduction

Value at risk (VaR) has been the most important market risk measure for two decades already. It is defined as a conditional quantile of the trading profit-and-loss (P&L) distribution at the end of a predefined time horizon. For example, a 10-day VaR at 99.0% confidence level is the loss that will *not* be exceeded at the end of the 10-day period with the probability of 99.0%. Although the VaR is widely used in practice, it does not perfectly describe the multifaceted nature of market risk. First, it is uninformative about the expected magnitude of losses beyond the calculated threshold level. To address this issue, Artzner et al. (1999), Acerbi and Tasche (2002a,b), and Rockafellar and Uryasev (2002) developed a new risk measure, i.e., the expected shortfall (ES), which represent the average loss beyond the VaR level. By construction, the ES is more conservative measure and it provides superior information about the tail risk that the VaR, which is precisely what matters the most for the market risk management. The second important methodological issue that is inherent to the VaR—and which has been largely overlooked in the literature—is the fact that it captures only the end-of-horizon effects, i.e., it does not provide any information about the possible losses before the expiration of the monitoring period. Kritzman and Rich (2002), Boudoukh et al. (2004), Rossello (2008), Bhattacharyya, Misra and Kodase (2009) and Bakshi and Panayotov (2010) studied a risk measure called intra-horizon value at risk (iVaR), which captures the "time dimension" of the market risk.[1] In particular, the iVaR is defined as a conditional quantile of the first-passage distribution (FPD) over a specified time horizon, hence it reflects the probability of incurring a loss of certain size at any point in time before (and including) the end of the monitoring period.

The intra-horizon risk was originally studied in Stulz (1996), pp. 20–22, in the context of cash flow risk in corporate risk management. Nevertheless, the notion of intra-horizon

[1] We emphasize that there is still no consensus in the literature regarding the name of the proposed risk measure. Boudoukh et al. (2004) and Bhattacharyya, Misra and Kodase (2009) use only the short name MaxVaR, and Bakshi and Panayotov (2010) call it the intra-horizon value at risk (abbreviated as VaR-I in their paper). We adopt the latter notation in our paper, but we label it with the short name iVaR.

risk is much broader and has many potential applications in finance. Kritzman and Rich (2002), pp. 92–93, mention the following examples: fiduciary asset management (due to intra-horizon performance provisions), loan agreements (due to mandatory reserves covenant), hedge-fund solvency (due to possible within-horizon withdrawals), regulatory requirements (due to the maintenance of the capital account), and securities lending (due to the required collateral deposit). Therefore, the intra-horizon risk is very important in a mark-to-mark environment where large trading losses in a short period of time can trigger margin calls and similar provisions.

In this paper, we consider the intra-horizon risk from the risk management perspective, and provide new important insights both from the theoretical and the empirical point of view. We build on the work of Bakshi and Panayotov (2010), who established a link between the VaR (the iVaR) and the expectation of a European (one-touch) digital payoff, and subsequently studied the two risk measures for several Lévy models.[2] To facilitate the computations with digital payoffs, they rely on an explicit finite difference scheme.[3] One of the main reasons for such an approach is the lack of alternative techniques that would allow studying of the first-passage distributions for a wide class of exponential Lévy processes, including both finite and infinite activity models, in a unified and consistent framework. The main theoretical contribution of our paper is that we propose an alternative solution to this problem, which is analytical and provides some additional insights about the iVaR.

First, we introduce a new jump-diffusion model for the asset price dynamics, which generalizes the mixed-exponential model (MEM) studied in Cai and Kou (2011). Generally, MEM models are attractive because exponential mixtures are flexible enough to arbitrarily closely approximate any continuous function on $[0, +\infty)$; e.g., see Botta and Harris (1986). Moreover, the support can be extended to the whole real line by considering separately

[2] Other models are also studied in the literature. Kritzman and Rich (2002) and Boudoukh et al. (2004) considered the Black-Scholes model and derived the closed-form expression for the probability of interim loss of a given magnitude. However, their modelling paradigm is rather oversimplified as it does not capture the salient features of asset returns, e.g., volatility clustering, negative skewness and excess kurtosis. On the other hand, Rossello (2008) and Bhattacharyya, Misra and Kodase (2009) studied the first-passage distribution in the double-exponential jump-diffusion setting and a GARCH model with non-normal innovations, respectively, using Monte Carlo methods.

[3] A digital (i.e., binary) payoff structure gives either one monetary unit or zero, conditionally on the occurrence of an event either at some specific date or within certain period of time in the future.

approximations on the positive and the negative real line. This is especially convenient for symmetric functions because it is enough to approximate only one half of the function. For example, Cai and Kou (2011), pp. 2077–2078, consider a MEM approximation of a normal distribution. However, their approximation procedure is directly applicable only to normal distributions with zero mean or mode.[4] In the case of a normal distribution with non-zero mean (or mode) ($\mu \neq 0$), the symmetry property cannot be exploited directly in the Botta and Harris (1986)'s framework, because the support of the left and right half of the normal distribution, i.e., $(-\infty, \mu)$ and $[\mu, +\infty)$, do not coincide with the support of the approximation function, i.e., the positive and the negative real line. Therefore, the two halves of the distribution have to be treated separately, and the procedure is computationally more expensive. Our model extends the standard setting by admitting the support of the form $[\mu, +\infty)$, with $\mu \in \mathbb{R}$, $|\mu| < +\infty$. For this reason we christen it the displaced mixed-exponential model (D-MEM). It can be verified that the D-MEM class is indeed very wide and flexible; it can approximate processes with completely monotone Lévy densities and jump-diffusion processes with arbitrary jump distributions. In the second step, following Leippold and Vasiljević (2015), we derive analytical results for the expectations of European and one-touch digital payoffs in the D-MEM setting using the Laplace-Carson transform (LCT). Moreover, we analytically disentangle the contributions of jumps and diffusion to the iVaR by studying the LCT of the first-passage time and the overshoot of the barrier level for the expectations of one-touch digital payoffs.

In their empirical study, Bakshi and Panayotov (2010) consider several popular Lévy models and stress out the importance of the model risk, i.e., the uncertainty about the correct model specification. We argue in this paper that the estimation risk, i.e., the uncertainty about the model parameters, might be even more important source of uncertainty. In particular, Bakshi and Panayotov (2010) follow the financial industry standard and calculate the VaR and the iVaR using the historical return time series. On the other hand, we estimate the two risk measures from the forward-looking perspective by using the options data, and the historical estimation plays the role of a benchmark

[4]The mean and the mode are identical for the class of normal distributions, and more generally for any symmetrical distribution.

in our empirical study. The rationale for our approach is the following. The existence of liquid options with different maturities and strikes makes it possible to study the option-implied probability distribution function and its moments for different investment horizons. Arguably, the option-based estimates are expected to exhibit superior forecasting performance than the historical estimates because they are more responsive to market changes due to their forward-looking nature.[5] Furthermore, the frequency of the historical returns data very often does not match exactly the time horizon that we are interested in, hence the estimated statistics or model parameters have to be adjusted accordingly. One way to achieve this goal is to use the time scaling, but this is possible only in some specific cases. Nevertheless, the time scaling adjustment can be completely circumvented by computing the option-implied risk measures. The term structure of option data makes it possible to at least closely match the option maturity with the target time horizon.

Although we argue that the option-implied statistics and model parameters are more informative about the future asset price dynamics and do not require time scaling, we also stress out that they are estimated under the risk-neutral measure. Therefore, using the option-implied estimates as direct inputs in calculations under the physical measure, e.g., the market risk management, would result in a theoretically inconsistent approach and, most likely, a poor empirical performance. However, the severity of this problem arguably depends on the time horizon. For example, Duffie and Pan (1997), pp. 10–11, claim that, in most markets, the distinction between the risk-neutral and the physical measure is negligible in short term. On the other hand, Boudoukh et al. (2004), p. 4, and Bakshi and Panayotov (2010), p. 23, assume that the expected return is equal to zero under the physical measure over a short time horizon. We adopt the latter assumption in our study and stress out that this approach necessitates a risk premium adjustment. To this end, we derive results for the change of measure in a general D-MEM setting, which guarantee the unique translation of the option-implied model parameters into the risk-adjusted (ex-ante physical) parameters. Overall, we work with one physical measure

[5] Since the seminal work of Latané and Rendleman (1976) and Breeden and Litzenberger (1978) many researchers have studied the informational content of risk-neutral distributions of asset returns, their statistical moments and other relevant parameters. An excellent overview of applications of option-implied information in forecasting is provided in Christoffersen, Jacobs and Chang (2013).

and two forward-looking measures.

Finally, to make our empirical results comparable to those of Bakshi and Panayotov (2010), we study the Merton (1976)'s jump-diffusion model (MJD), the finite-moment log-stable model (FMLS) of Carr and Wu (2003), and the Carr-Geman-Madan-Yor model (CGMY) of Carr et al. (2002). Additionally, we consider the variance-gamma model of Madan and Seneta (1990). All listed models can be approximated by the D-MEM class, hence we are able to analyze them consistently in a unified framework using our theoretical results. The model parameters are estimated separately from the historical return time series and the short-term American put options on the S&P 100 index spanning the period from March 2001 until 2014. Using a major index in the empirical study is particularly appealing because of the data availability, and due to the fact that broad indices are often used as proxies for risk factors. Our empirical results for 10-day VaR and iVaR estimates at the confidence levels of 99.0% and 99.9% indicate significantly higher values under the forward-looking measures relative to the physical measure. A simple backtesting procedure shows that, irrespectively of the model used, the risk-adjusted VaR and iVaR estimates are much more perceptive and responsive to asset price fluctuations, as produce superior results relative to the historical estimates. We conclude that, at least within the scope of our study, the importance of estimation risk surpasses the importance of the model risk. For this reason, we think that, whenever option data is available, the option-implied estimates of risk measures should not be neglected in practice.

The paper is structured as follows. In Section 2, we introduce the displaced mixed-exponential model and the associated change of measures and we provide examples of D-MEM approximations of certain Lévy models. In Section 3 we derive European and one-touch digital options and discuss their link to the iVaR. Furthermore, we presesent the theoretical results for the first-passage disentanglement of the jump contribution from the diffusion contribution to the iVaR. In Section 4, we describe the data treatment and summarize the calibration and the model performance results. Our empirical findings for the VaR, the iVaR, and the FPD (under the historical and the risk-adjusted measure) are discussed in Section 5. We conclude in Section 6. All proofs, tables and figures are given

in the Appendix.

2 Displaced mixed-exponential model (D-MEM)

2.1 The model set-up

Let $(\Omega, \mathcal{F}, \mathbb{F} = \{\mathcal{F}_t, t \geq 0\}, \mathbb{P})$ be a a filtered probability space which satisfies the usual assumptions, where $\mathcal{F}_t = \sigma(W_s, N_s; s \leq t, \{V_j\})$. The stochastic process $\{W_t, t \geq 0\}$ is a standard Brownian motion. The Poisson process $\{N_t, t \geq 0\}$ is characterized by jump intensity parameter $\lambda \in \mathbb{R}_0^+$, and $\{Y_i := \log(V_i) : i = 1, 2, ...\}$ represents a sequence of independent and identically distributed (i.i.d.) displaced mixed-exponential random variables. The Lévy density of D-MEM is

$$\nu(y) = \lambda_+ \sum_{i=1}^{m} p_i \eta_i e^{-\eta_i (y-\xi)} \mathbb{1}_{\{y \geq \xi\}} + \lambda_- \sum_{j=1}^{n} q_j \theta_j e^{\theta_j (y-\xi)} \mathbb{1}_{\{y < \xi\}}. \tag{1}$$

The displacement parameter ξ is the mode of the Lévy density. It represents the jump magnitude at which a mixture of standard exponential distributions (the right half of D-MEM distribution) is glued back-to-back to a mixture of "y-axis-mirrored" exponential distribution (the left half of D-MEM distribution), as it is graphically exemplified in Panels A and C in Figure 1. Henceforth we refer to the two types of jumps as ξ^+ and ξ^--jumps, respectively.

[Insert Figure 1 about here]

The parameters $\lambda_+ \in \mathbb{R}_0^+$ and $\lambda_- \in \mathbb{R}_0^+$ represent the respective (finite-activity) jump intensities of the two jump mixtures. The total jump activity is therefore $\lambda = \lambda_+ + \lambda_-$, and the jump size probability distribution function (p.d.f.) is defined as $f_Y(y) := \nu(y)/\lambda$. The parameters $\{\eta_i \in (1, +\infty) : i = 1, ..., m\}$ are the magnitude parameters of ξ^+-jumps. Similarly, the set $\{\theta_j \in (0, +\infty) : j = 1, ..., n\}$ represents the magnitude parameters of ξ^--jumps.[6] Without loss of generality we assume that $\eta_1 < \eta_2 < ... < \eta_m$ and

[6] The average jump size of a given type is an inverse of the corresponding magnitude parameter.

$\theta_1 < \theta_2 < ... < \theta_n$. Finally, the mixing weights $\{p_i \in \mathbb{R} : i = 1, ..., m\}$ and $\{q_j \in \mathbb{R} : j = 1, ..., n\}$ satisfy equations: $\sum_{i=1}^{m} p_i = 1$ and $\sum_{j=1}^{n} q_j = 1$. Since we allow weights to be negative, certain conditions need to be satisfied to ensure that the function $f_Y(y)$ represents a p.d.f. Steutel (1967) showed that the necessary conditions are: $p_1 > 0$, $q_1 > 0$, $\sum_{i=1}^{m} p_i \eta_i \geq 0$, and $\sum_{j=1}^{n} q_j \theta_j \geq 0$. On the other hand, Bartholomew (1969) showed that the sufficient conditions are: $\sum_{i=1}^{m'} p_i \eta_i \geq 0$ for all $m' = 1, 2, ..., m$, and $\sum_{j=1}^{n'} q_j \theta_j \geq 0$ for all $n' = 1, 2, ..., n$.

The asset price dynamics under the physical probability measure $\mathbb{P}$ follows a displaced mixed-exponential jump-diffusion process

$$\frac{dS_t}{S_{t^-}} = \mu dt + \sigma dW_t + d\left(\sum_{i=1}^{N_t}(V_i - 1)\right). \tag{2}$$

The drift $\mu \in \mathbb{R}$, and the volatility $\sigma \in \mathbb{R}^+$ are assumed to be constant. It follows from the Itô lemma that the log-price process $\{X_t := \log S_t, t \geq 0\}$ is given by

$$X_t = X_0 + \bar{\mu} t + \sigma W_t + \sum_{i=1}^{N_t} Y_i, \quad X_0 := \log S_0, \tag{3}$$

where $\bar{\mu} := \mu - \lambda\zeta - \frac{\sigma^2}{2}$ represents the compensated drift term. The average jump size is

$$\zeta := \mathbb{E}\left[e^{Y_1} - 1\right] = \left(\frac{\lambda_+}{\lambda}\sum_{i=1}^{m}\frac{p_i\eta_i}{\eta_i - 1} + \frac{\lambda_-}{\lambda}\sum_{j=1}^{n}\frac{q_j\theta_j}{\theta_j + 1}\right)e^{\xi} - 1. \tag{4}$$

The cumulant generating function (c.g.f.) of the log-price process $\{X_t, t \geq 0\}$ is defined for any $u \in (-\theta_1, \eta_1)$ as

$$\Psi(u) := \frac{1}{t}\log\mathbb{E}\left[e^{uX_t}\right] = \mu u + \frac{1}{2}\sigma^2 u^2 + \lambda\left(\left(\frac{\lambda_+}{\lambda}\sum_{i=1}^{m}\frac{p_i\eta_i}{\eta_i - u} + \frac{\lambda_-}{\lambda}\sum_{j=1}^{n}\frac{q_j\theta_j}{\theta_j + u}\right)e^{u\xi} - 1\right). \tag{5}$$

We note that several popular jump-diffuson models can be nested in the D-MEM class. In particular, any MEM model can be interpreted as the corresponding D-MEM model without displacement ($\xi = 0$). Moreover, zero displacement parameter characterizes also

the class of hyper-exponential models (HEM), with the additional constraint that the mixing weights $\{p_i\}_{i=1,\dots,m}$ and $\{q_j\}_{j=1,\dots,n}$ in (1) have to be strictly positive. Finally, double-exponential models (DEM) represent a subclass of HEM models (with $n = m = 1$), and therefore can also be nested in the D-MEM family.[7]

Cai (2009), Lemma 2.1, pp. 128–129, proved for the class of hyper-exponential models that the characteristic equation

$$\Psi(u) = \alpha, \ \alpha \in \mathbb{R}^+, \tag{6}$$

which is polynomial and has exactly $(n + m + 2)$ distinct real roots. Nevertheless, one cannot obtain the roots in analytic form for an arbitrary choice of m and n. Already in the case of double-exponential models one has to solve a quartic equation, and if we allow for additional types of positive and negative jumps the problem becomes analytically intractable. Furthermore, Cai and Kou (2011), Theorem 3.1, p. 2071, showed for the MEM class that, for sufficiently large α, the characteristic equation (6) has also $(n+m+2)$ real roots. Similarly, the number of positive and negative characteristic roots in a D-MEM model depends on the constant α. However, any further generalization of the analytical results for HEM and MEM characteristic roots to the case of D-MEM class of jump-diffusion models is a much more challenging task. If the displacement parameter ξ is non-zero, the expression (6) becomes an exponential-polynomial equation, which is difficult to analyze and solve analytically in a general setting. Even if some additional assumptions are imposed, e.g., the number of $\xi^{\pm}$-jumps is fixed in advance, one has to carefully investigate different model specifications. The most general statement that we can make regarding the roots of a D-MEM (exponential-polynomial) characteristic equation is that there exist $\hat{m} := \hat{m}(\alpha) \leq m + 1$ positive roots $\{\beta_{i,\alpha}\}_{i=1,\dots,\hat{m}}$, and $\hat{n} := \hat{n}(\alpha) \leq n + 1$

[7] HEM class of models was studied in the following papers: Lipton (2002), Cai (2009, 2011), Cai, Chen and Wan (2009), Crosby, Le Saux and Mijatović (2010), Jeannin and Pistorius (2010), Boyarchenko and Boyarchenko (2011), Cai and Kou (2012), Hofer and Meyer (2013), Yin, Shen and Wen (2013), Cai and Sun (2014). The main references for the DEM models are: Kou (2002), Kou and Wang (2003, 2004), Sepp (2004), Kou, Petrella and Wang (2005), AitSahlia and Runnemo (2007), Ramezani and Zeng (2007), Toivanen (2008), Wong and Lau (2008), Bayraktar and Xing (2009, 2011), Cai, Chen and Wan (2010), Albrecher, Kortschak and Zhu (2012) and Fuh, Luo and Yen (2013).

negative roots $\{\gamma_{i,\alpha}\}_{j=1,\ldots,\hat{n}}$, which satisfy the ordering relation

$$-\infty < \gamma_{\hat{n},\alpha} < \cdots < \gamma_{2,\alpha} < \gamma_{1,\alpha} < 0 < \beta_{1,\alpha} < \beta_{2,\alpha} < \cdots < \beta_{\hat{m},\alpha} < +\infty. \tag{7}$$

Therefore, the characteristic root finding problem for a D-MEM model can only be tackled numerically. Some examples and intuition for the behavior of c.g.f. (5) and the roots of the equation (6) for different types of D-MEM models are presented in Panels B and D in Figure 1.

2.2 The change of measure

The market incompleteness of Lévy models represents one of the major challenges for their practical applications. However, this problem can be solved by defining the change of measure via the Esscher (1932)'s transform, which can be interpreted as a generalization of the Cameron-Martin-Girsanov change of measure. Gerber and Shiu (1994) proved that the Esscher transform approach can be justified within a rational expectations framework where the representative agent is characterized by a certain type of utility function. The main implication of this result for the option pricing is that there exists a risk-neutral measure such that, in equilibrium, options are priced as expectations of their discounted payoffs. Chan (1999) and Miyahara (1999) provided an alternative interpretation of the Esscher transform in terms of the minimum entropy martingale measure.[8] Therefore, we work along the same lines and introduce the change of measure via the Esscher transform, i.e., the Radon-Nikodým derivative process is defined as

$$Z_t(\vartheta) := \left.\frac{d\mathbb{Q}^{\vartheta}}{d\mathbb{P}}\right|_{\mathcal{F}_t} = \frac{e^{\vartheta X_t}}{\mathbb{E}\left[e^{\vartheta X_t}\right]}. \tag{8}$$

The expectation $\mathbb{E}[\cdot]$ is computed under the physical probability measure $\mathbb{P}$. The Esscher transform parameter is denoted by ϑ, and the process (8) is well defined for $\vartheta \in (-\theta_1, \eta_1)$.

[8] For a detailed account on the Esscher transform in mathematical finance we refer an interested reader to Hubalek and Sgarra (2006) and the references therein. Additionally, some important examples of Esscher transform applications in option pricing with Lévy processes can be found in, e.g., Milne and Madan (1991), Eberlein and Keller (1995), Kou (2002), Kou and Wang (2004), Carr and Wu (2004), Kou, Petrella and Wang (2005), Wu (2006), Cai (2011), and Fabozzi, Leccadito and Tunaru (2014).

Theorem 1 proves that the Esscher transform admits a structure-preserving change of measure for D-MEM processes. Moreover, the risk-neutral probability measure $\mathbb{Q}^{\vartheta}$ is uniquely identified by choosing the value of ϑ such that the forward no-arbitrage constraint is satisfied, i.e., the discounted and process $\left\{e^{-rt}S_t, t \geq 0\right\}$ is a $\mathbb{Q}^{\vartheta}$-martingale.

Theorem 1 (**Risk-netural dynamics**).

The risk-neutral dynamics of the log-price process in the displaced mixed-exponential model (1)–(3) is given by

$$X_t = X_0 + \bar{r}t + \sigma W_t^* + \sum_{i=1}^{N_t^*} Y_i^*, \quad X_0 := \log S_0. \tag{9}$$

The processes $\{W_t^*, t \geq 0\}$ *and* $\{N_t^*, t \geq 0\}$ *represent the Brownian motion and the Poisson process under the risk-neutral measure* $\mathbb{Q}^{\vartheta}$*, respectively. The compensated drift term is* $\bar{r} := r - \frac{\sigma^2}{2} - \lambda^*\zeta^*$*, where parameter* r *denotes the risk-free rate, and* λ^* *and* $\zeta^* := \left(\frac{\lambda_+^*}{\lambda^*}\sum_{i=1}^m \frac{p_i^*\eta_i^*}{\eta_i^*-1} + \frac{\lambda_-^*}{\lambda^*}\sum_{j=1}^n \frac{q_j^*\theta_j^*}{\theta_j^*+1}\right)e^{\xi^*} - 1$ *represent the jump intensity and the expected jump size under the new measure, respectively. The* $\mathbb{Q}^{\vartheta}$*-parameters can be computed as follows:*

$$\begin{cases} \sigma^* = \sigma, \ \xi^* = \xi, \\ \lambda_+^* = \lambda_+ \sum_{i=1}^m \dfrac{p_i\eta_i}{\eta_i - \vartheta} e^{\vartheta\xi}, \quad \lambda_-^* = \lambda_- \sum_{j=1}^n \dfrac{q_j\theta_j}{\theta_j + \vartheta} e^{\vartheta\xi}, \ \lambda^* = \lambda_+^* + \lambda_-^*, \\ p_i^* = \dfrac{\frac{p_i\eta_i}{\eta_i - \vartheta}}{\sum_{i=1}^m \frac{p_i\eta_i}{\eta_i - \vartheta}}, \quad \eta_i^* = \eta_i - \vartheta, \quad \text{for } i = 1, 2, ..., m, \\ q_j^* = \dfrac{\frac{q_j\theta_j}{\theta_j + \vartheta}}{\sum_{j=1}^n \frac{q_j\theta_j}{\theta_j + \vartheta}}, \quad \theta_j^* = \theta_j + \vartheta, \quad \text{for } j = 1, 2, ..., n. \end{cases} \tag{10}$$

The Esscher transform parameter ϑ *is the unique solution of the equation*

$$\mu - r - \lambda\zeta + \vartheta\sigma^2 + \Psi_J(\vartheta + 1) - \Psi_J(\vartheta) = 0, \tag{11}$$

where $\Psi_J(a) := \mathbb{E}\left[e^{a\sum_{i=1}^{N_t} Y_i}\right] = \lambda\left(\left(\frac{\lambda_+}{\lambda}\sum_{i=1}^m \frac{p_i\eta_i}{\eta_i - a} + \frac{\lambda_-}{\lambda}\sum_{j=1}^n \frac{q_j\theta_j}{\theta_j + a}\right)e^{a\xi} - 1\right)$ *is the c.g.f. of the jump part (i.e., the compound Poisson process).*

Although we have introduced the change of measure following the standard approach in the literature, i.e., going from the physical to the risk-neutral probability measure, it is actually the opposite direction that is of primary interest in this paper. Our goal is to obtain the VaR and the iVaR estimates by calibrating our models to option data, and subsequently accounting for the risk premium by transforming the obtained parameters from the risk-neutral to the physical world. To distinguish the option-implied set of parameters which is adjusted for the risk premium from the set of parameters estimated directly under the physical measure, we refer to them as the risk-adjusted (or the ex-ante physical) and the historical parameters, respectively. Although we have introduced the Esscher transform for D-MEM processes following the standard approach in the literature and starting from the physical world dynamics, it is actually the opposite direction of the change of measure which is of primary interest in our paper. The risk-adjusted parameters are computed by adopting the assumption of Boudoukh et al. (2004) and Bakshi and Panayotov (2010) that the risk-adjusted drift is equal to zero ($\mu = 0$), and reversing the procedure for the change of measure in Theorem 1. We denote the risk-neutral measure by $\mathbb{Q}$ and the risk-adjusted measure by $\mathbb{Q}^{\vartheta}$, where ϑ now represents the Esscher transform parameter corresponding to the "backward" change of measure, i.e., from $\mathbb{Q}$ to $\mathbb{Q}^{\vartheta}$. Furthermore, we adjust accordingly the notation in the expression (10); the $\mathbb{Q}^{\vartheta}$-parameters are henceforth designated by the asterisk sign in the superscript. It follows directly that the Esscher transform parameter ϑ is a function of the risk-neutral parameters, and it can be determined as the unique solution of the equation

$$r - \lambda\zeta + \vartheta\sigma^2 + \Psi_J(\vartheta + 1) - \Psi_J(\vartheta) = 0, \tag{12}$$

which, in turn, allows us to compute the risk-adjusted D-MEM parameters. Similarly to the characteristic equation (6), the equation (12) can be solved only numerically for more involved model specifications.

2.3 D-MEM approximations of exponential Lévy processes

In this section, we provide expressions for D-MEM approximations of several exponential Lévy models. They can be broadly classified in two groups: finite-activity jump-diffusion processes and completely monotone Lévy processes of infinite-activity. In particular, we focus on the models that we consider in our empirical study, i.e., MJD, FMLS, VG, and CGMY.

2.3.1 Finite-activity jump-diffusion models: MJD

We have already mentioned in Section 2 that DEM, HEM, and MEM models can be nested within the D-MEM class. This means that their respective D-MEM approximations are exact. On the other hand, the D-MEM approximation is not so trivial for models with a "non-exponential" distribution of jump sizes. In particular, we consider the well known jump-diffusion model of Merton (1976). The log-price dynamics is described by the equation (3), and jumps are assumed to be normally distributed, i.e., $Y \overset{\text{i.i.d.}}{\sim} \mathcal{N}(\mu_J, \sigma_J^2)$. Therefore, the Lévy density is given by

$$\nu_{\text{MJD}}(y) = \frac{\lambda}{\sqrt{2\pi\sigma_J^2}} \exp\left(-\frac{(y-\mu_J)^2}{2\sigma_J^2}\right), \tag{13}$$

and the characteristic function is

$$\begin{aligned} \varphi_{\text{MJD}}(u) :&= \mathbb{E}\left[\exp(iuX_t)\right] \\ &= \exp\left(iu\mu t - \frac{u^2\sigma^2 t}{2} + \lambda t\left(\exp\left(iu\mu_J - \frac{u^2\sigma_J^2}{2}\right) - 1\right)\right). \end{aligned} \tag{14}$$

Cai and Kou (2011), pp. 2077–2078, provided a MEM approximation of normally distributed variable $Y \overset{\text{i.i.d.}}{\sim} \mathcal{N}(0, 0.01^2)$. However, we pointed out in Section 1 that displaced mixed-exponential distributions are better suited for approximations of normal distributions with non-zero mean/mode. Using a simple change of variables, we demonstrate that a D-MEM approximation of a normal distribution can be transformed into a MEM approximation.

Let's assume that the MEM approximation of the p.d.f. of a normally distributed random variable $Y \overset{\text{i.i.d.}}{\sim} \mathcal{N}(0, \sigma_J^2)$ is given by

$$f_Y(y) \approx 0.5 \sum_{i=1}^{m} p_i \eta_i e^{-\eta_i |y|}. \tag{15}$$

The r.h.s. is a special case of the general expressions for MEM and D-MEM probability distribution functions given in equation (1). In addition to the zero displacement, the number of positive exponentials is equal to the number of negative exponentials ($m = n$), and the parameters of the positive and the negative exponential functions and their corresponding mixing weights are component-wise identical, i.e., $\theta_i = \eta_i$ and $p_i = q_i$ for all $i = 1, 2, ..., m$, respectively. Furthermore, the mixture of exponential distributions is pre-multiplied by a constant which can be translated in the condition $\lambda_+/\lambda = \lambda_-/\lambda = 0.5$, i.e., the activity rates of positive and negative jumps are equal. The reason for all these restrictions on MEM parameters is the symmetry property of normal distributions. Once the distribution of the random variable Y is fitted with desired accuracy, we can derive the approximation for any normally distributed variable $\tilde{Y} \overset{\text{i.i.d.}}{\sim} \mathcal{N}(\tilde{\mu}_J, \tilde{\sigma}_J^2)$. The two random variables can be expressed in terms of a standard normal variable $Z \overset{\text{i.i.d.}}{\sim} \mathcal{N}(0, 1)$, i.e., $Y = \sigma_J Z$ and $\tilde{Y} = \tilde{\mu}_J + \tilde{\sigma}_J Z$. Therefore, we have that $\tilde{Y} = \tilde{\mu}_J + \frac{\tilde{\sigma}_J}{\sigma_J} Y$. Simple algebra gives us the expression for the D-MEM approximation for the distribution of $\mathcal{N}(\tilde{\mu}_J, \tilde{\sigma}_J^2)$ via the MEM approximation (15):

$$f_{\tilde{Y}}(\tilde{y}) \approx 0.5 \sum_{i=1}^{m} \tilde{p}_i \tilde{\eta}_i e^{-\tilde{\eta}_i |\tilde{y} - \tilde{\mu}_J|}, \tag{16}$$

with $\tilde{\eta}_i = \frac{\sigma_J}{\tilde{\sigma}_J} \eta_i$ and $\tilde{p}_i = p_i$ for $i = 1, 2, ..., m$. Expectedly, the displacement parameter is $\xi = \tilde{\mu}_J$. Finally, from the perspective of Merton's jump-diffusion model, the diffusion parameter σ and the jump intensity λ remain unchanged, which is justified by the fact that the D-MEM approximation (16) affects only the distribution of jump sizes.

2.3.2 Completely monotone Lévy processes: FMLS, VG, and CGMY

All pure-jump Lévy processes studied in this paper, i.e., FMLS, VG, and CGMY, are completely monotone. It is precisely this property that allows us to approximate the considered Lévy processes with hyper-exponential models. In particular, a Lévy density $\nu : (0, +\infty) \to \mathbb{R}$ is said to be completely monotone if it for all $k \in \mathbb{N}_0^+$ it is of class $\mathcal{C}^\infty$ and holds that $(-1)^k d^k \nu(y)/dy^k > 0$ for all $y > 0$; e.g., see Sato (1999), p. 388.[9] Furthermore, the Bernstein's theorem ensures that a Lévy density is completely monotone if and only if it can be decomposed as

$$\nu(y) = \mathbb{1}_{\{y<0\}} \int_{-\infty}^{0} e^{-vy} \rho_-(dv) + \mathbb{1}_{\{y>0\}} \int_{0}^{+\infty} e^{-vy} \rho_+(dv), \tag{17}$$

where $\rho_-(dv)$ and $\rho_+(dv)$ are Radon measures on intervals $(-\infty, 0)$ and $(0, +\infty)$, respectively, such that the two integrals are finite. In a nutshell, this means that the arrival rate of jumps is decreasing with the jump size. If the integrals on the r.h.s. of the equation (17) are discretized, the completely monotone Lévy density $\nu(\cdot)$ is approximated by a finite mixture of exponential densities. Moreover, jumps with expected size smaller then certain threshold, i.e., jumps with magnitudes closed to zero, can be approximated by a diffusion process. Based on this approximation, Asmussen, Madan and Pistorius (2007) infer that completely monotone jump models can be approximated by hyper-exponential jump-diffusion models, which are a subset of the displaced mixed-exponential class.

As an example of the hyper-exponential approximation of a completely monotone Lévy model, we consider the CGMY process of Carr et al. (2002). It is a pure-jump process, and its Lévy density is given by the exponentially dampened power law

$$\nu_{CGMY}(y) = C \left(\frac{e^{-G|y|}}{|y|^{1+Y}} \mathbb{1}_{\{y<0\}} + \frac{e^{-My}}{y^{1+Y}} \mathbb{1}_{\{y>0\}} \right), \tag{18}$$

[9] This definition can be easily extended to the whole real line. The condition for the complete monotonicity then becomes $(-1)^k d^k \nu(|y|)/dy^k > 0$ for $y \in (-\infty, +\infty)$.

and its characteristic function is

$$\begin{aligned}\varphi_{\mathrm{CGMY}}(u) :&= \mathbb{E}\left[\exp(iuX_{\mathrm{CGMY}}(t))\right] \\ &= \exp\left(iu\omega t + tC\Gamma(-Y)\left((M-iu)^Y - M^Y + (G+iu)^Y - G^Y\right)\right),\end{aligned} \tag{19}$$

where $\omega := -C\Gamma(-Y)((M-1)^Y - M^Y + (G+1)^Y - G^Y)$ represents the convexity adjustment, and $\Gamma(\cdot)$ denotes the mathematical gamma function. The parameter $C \in \mathbb{R}^+$ represents the jump intensity. The parameters $G \in \mathbb{R}_0^+$ and $M \in \mathbb{R}_0^+$ are exponential decay parameters of negative and positive jumps, respectively. Depending on their relative values, the model can generate positive, negative or zero skewness. The parameter Y is especially interesting because it characterizes the so called "fine structure" of asset returns, i.e., it describes the behavior of the Lévy density in the neighborhood of zero.[10] Following the idea of Asmussen, Madan and Pistorius (2007), Section 2.1, pp. 85–87, and Jeannin and Pistorius (2010), Section 2, pp. 631–632, our starting point is the identity

$$\frac{1}{y^{1+Y}} = \frac{1}{\Gamma(1+Y)} \int_0^{+\infty} u^Y e^{-uy} du, \tag{20}$$

which holds for all $Y \in \mathbb{C} \setminus \{-2, -3, -4, ...\}$. This expression follows directly from the definition of the gamma function. Discretization of the integral on the r.h.s. of (20) yields

$$\frac{1}{y^{1+Y}} \approx \frac{1}{\Gamma(1+Y)} \sum_{i=1}^{N-1} u_i^Y e^{-u_i y}(u_{i+1} - u_i). \tag{21}$$

The partitioning $\Pi(N) := (u_i)_{i=1,2,...,N-1}$ of the interval $(0, +\infty)$ is such that $\Delta_{\Pi(N)} \to 0$ when $N \to \infty$, with the norm defined as $\Delta_{\Pi(N)} = \max_{1 \le i \le N-1} |u_{i+1} - u_i|$. Therefore, a completely monotone process can be approximated with arbitrary accuracy by choosing appropriate partition of the integration interval. For example, CGMY density (18) can

[10] A CGMY process is completely monotone if $Y \in (-1, 2)$. Furthermore, for $Y < 0$ the process is of finite activity; for $Y \in (0, 1)$ it is characterized by infinite activity and finite variation, and for $Y \in (1, 2)$ it has infinite variation, but finite quadratic variation. For more details about the CGMY process see, e.g., Koponen (1995), Boyarchenko and Levendorskiĭ (2000) and Carr et al. (2002).

be approximated as

$$\begin{aligned}\nu_{CGMY}(y) \approx \frac{C}{\Gamma(1+Y)} \sum_{i=1}^{N^+-1} w_i^+ e^{-(M+u_i)y} \mathbb{1}_{\{y>0\}} \\ + \frac{C}{\Gamma(1+Y)} \sum_{j=1}^{N^--1} w_j^- e^{-(G+v_j)|y|} \mathbb{1}_{\{y<0\}},\end{aligned} \tag{22}$$

where $w_i^+ := u_i^Y(u_{i+1}-u_i)$ for $i = 1, 2, ..., N^+$, and $w_j^- := v_j^Y(v_{j+1}-v_j)$ for $j = 1, 2, ..., N^-$. We implicitly introduced the partitioning $U(N^+) := (u_i)_{i=1,2,...,N^+-1}$ of the interval $(0, +\infty)$, as well as the partition $V(N^-) := (v_j)_{j=1,2,...,N^--1}$ of the interval $(-\infty, 0)$. One can easily check that the r.h.s. of the expression (22) corresponds to the D-MEM Lévy density (1) with the following parameters: $m = N^+ - 1$, $n = N^- - 1$, $\eta_i = M + u_i$ and $p_i = w_i^+/\eta_i$ for $i = 1, 2, ..., m$, $\theta_j = G + v_j$ and $q_j = w_j^-/\theta_j$ for $j = 1, 2, ..., n$, $\lambda_+ = \tilde{C}\sum_{i=1}^{N^+-1} p_i$ and $\lambda_- = \tilde{C}\sum_{j=1}^{N^--1} q_j$, where $\tilde{C} = C/\Gamma(1+Y)$.[11] Therefore, depending on the discretization and the truncation error, which are determined by the choice of the partition of the positive and negative semi-axes, we can obtain an arbitrarily accurate approximation of the CGMY density.

In practical applications, Asmussen, Madan and Pistorius (2007) fix in advance the number of components in the mixture and their respective exponential decay parameters. Subsequently, they minimize a distance between the two Lévy densities by optimally choosing the partition of the integration intervals. Jeannin and Pistorius (2010) follow almost identical procedure, except that they optimize the mixing weights.[12] Nevertheless, the approximation derived in (22) implies that there exists a structural relation between the exponential decay parameters and the corresponding mixing weights. Hence, the total number of jumps and the values of the model parameters are in fact determined by the chosen partition. Consistently with the theoretical results presented in equations (20)–(22), and simultaneously avoiding a computationally burdensome numerical optimization

[11] We note that, in the D-MEM approximation of a CGMY process, the displacement parameter is equal to zero. More generally, the displacement has to be zero for any model with infinite activity; otherwise, the integral of the Lévy density would not exist.

[12] The number of exponential terms in the mixture varies between 5 and 7 in Asmussen, Madan and Pistorius (2007) and Jeannin and Pistorius (2010).

without loss of accuracy, we make a trade-off by choosing a larger number of exponential terms.[13] However, for the remaining steps in our exercise, e.g., for the approximation of small jumps by a diffusion, we follow closely procedure outlined in Asmussen, Madan and Pistorius (2007) and Jeannin and Pistorius (2010) since it ensures the weak convergence of the constructed sequence of HEM processes to the target Lévy process.

In addition to the CGMY model we consider two other popular pure-jump models, i.e., the VG model of Madan and Seneta (1990) and the FMLS model of Carr and Wu (2003). Both models are special cases of CGMY. The Lévy density of a VG process is obtained by setting the fine structure parameter to zero in the equation (18). On the other hand, the FMLS process is a spectrally negative Lévy process, i.e., positive jumps are completely excluded, and the exponential decay parameter of negative jumps is set to zero. We do not explicitly state the Lévy measures and the characteristic functions of VG and FMLS processes because they can be inferred directly from (18) using the aforementioned restrictions.

3 Theoretical results

3.1 VaR and iVaR: The connection with digital payoffs

Bakshi and Panayotov (2010) established a connection between the iVaR and an expectation of a one-touch digital payoff. In this section, we first summarize their finding, and also develop an analogous procedure to recover the VaR from an expectation of a European digital payoff.[14]

The iVaR is defined as a conditional quantile of the first-passage distribution (FPD)

[13] In particular, we use 50 (non-degenerate) exponential terms in the mixture. Our numerical tests show that the suggested procedure is generally fast and stable. It is important to stress out that a detailed investigation of the three approximation approaches described in this section is a separate research topic. The algorithms outlined here are by no means the major concern of our paper, and the sole purpose of this section is to briefly describe our approach and related it to the relevant papers. Admittedly, there also exist other approaches in the literature, e.g., Crosby, Le Saux and Mijatović (2010) and Hackmann and Kuznetsov (2014). Nonetheless, we find that our modification of Asmussen, Madan and Pistorius (2007) and Jeannin and Pistorius (2010) works sufficiently well for our application.

[14] Bakshi and Panayotov (2010), Section 6, p. 26, do not use the digital options framework to infer the VaR. They instead compute the conditional quantiles of the p.d.f. numerically using the Fourier inversion.

of the asset return process; see Section 3 in Bakshi and Panayotov (2010), p. 23. The cumulative distribution function (c.d.f.) of the FPD can be computed as the conditional expectation that the log-price process $\{X_u, t \leq u \leq T\}$ will drop below certain pre-specified level $\kappa := \log(K)$, i.e.,

$$P(X_t, \tau) := \mathbb{E}^x \left[\mathbb{1}_{\{X_u < \kappa\}}, t < u \leq T \right], \tag{23}$$

where $\tau := T - t$ represents the remaining time before the expiry of the monitoring period, and the value of the log-price process at time t is given by x. The iVaR calculations bring about the payoff structure which is identical to that of the one-touch digital down-and-in put options.[15] However, the expectation in the equation (23) is not taken under the risk-neutral measure. Moreover, even if it were the case, there is no discounting (at the risk-free rate). Therefore, we emphasize that the expression for the c.d.f. of the FPD resembles, but it is *not*, an option pricing problem.

To ease the notation, we first drop the adjective 'down-and-in', as this is the only type of digital payoffs that we consider in this paper. Second, we introduce the name *optionette* to designate the expectation (23) and alike, e.g., we use the expressions 'to calculate the (undiscounted) expectation of the one-touch digital put payoff' and 'to price the one-touch digital put optionette' interchangeably. We purposefully chose the name containing the word 'option' because, in our particular setting which assumes the zero expected return under the pricing measure, the c.d.f. of the FPD (as well as the c.d.f. of the end-of-horizon asset return distribution, as we will see in the case of VaR) is a martingale.[16] The differences in the probability measure and the discounting clearly introduce a wedge between the options from the optionettes, however the rationale behind their respective calculations is the same, i.e., the martingale method.

[15] Alternatively, one can study the case when the barrier level is above the current asset price level, i.e., the digital up-and-in call payoff structure. We focus in our study on the downside risk of the P&L distribution, i.e., we consider only long positions in the asset.

[16] In the empirical part, we will look into two different physical-world measures, i.e., the historical measure $\mathbb{P}$ (which is obtained by calibrating the models to the historical returns data), and the risk-adjusted measure $\mathbb{Q}^{\vartheta}$ (which is obtained by calibrating the models to the options data, and subsequently applying the risk neutralization procedure).

It follows from the Feynman-Kac theorem that the option price can be computed by solving the PIDE

$$-\frac{\partial P}{\partial \tau}(x,\tau)+\frac{\sigma^2}{2}\frac{\partial^2 P}{\partial x^2}(x,\tau)+\bar{\varrho}\frac{\partial P}{\partial x}(x,\tau)+\int_{-\infty}^{+\infty}[P(x+y,\tau)-P(x,\tau)]\nu(y)dy=0, \tag{24}$$

where $\bar{\varrho}$ denotes the compensated drift term of the log-price process under some pre-specified physical measure, and the Lévy measure $\nu(\cdot)$ is defined in the equation (1). The boundary and the initial conditions are:

$$\begin{cases} \lim\limits_{x\uparrow+\infty} P(x,\tau) & = 0, \\ \lim\limits_{x\downarrow\kappa} P(x,\tau) & = 1, \\ \lim\limits_{\tau\downarrow 0} P(x,\tau) & = \mathbb{1}_{\{x<\kappa\}}. \end{cases} \tag{25}$$

The iVaR (with the monitoring horizon τ and the confidence level χ) can be computed as

$$\text{iVaR}(\tau,\chi)=S_t-e^{\underline{\kappa}}, \quad \text{given that} \quad P(x,\tau;\underline{\kappa})=1-\chi. \tag{26}$$

Therefore, the iVaR can be interpreted as the difference between the current asset price S_t and the implied $(1-\chi)$-quantile level $\underline{K}=\exp(\underline{\kappa})$ of the c.d.f. of the FPD estimated over the monitoring period τ.

On the other hand, the VaR is related to the c.d.f. of the asset return process at the end of the monitoring period τ, which can be computed as an expectation of the European digital put payoff:

$$p(X_t,\tau)=\mathbb{E}^x\left[\mathbb{1}_{\{X_T<\kappa\}}\right], \tag{27}$$

where κ should be interpreted as the strike price rather than the barrier level. Similarly to the case of one-touch digital put optionette, the dynamics of a European digital put optionette price satisfies the equation (24). However, the boundary and the initial

conditions are

$$\begin{cases} \lim\limits_{x\uparrow+\infty} p(x,\tau) &= 0, \\ \lim\limits_{x\downarrow-\infty} p(x,\tau) &= 1, \\ \lim\limits_{\tau\downarrow 0} p(x,\tau) &= \mathbb{1}_{\{x<\kappa\}}. \end{cases} \tag{28}$$

Therefore, the VaR can be computed as the difference between the current asset price S_t and the implied $(1-\chi)$-quantile level $\overline{K} = \exp(\overline{\kappa})$ of the c.d.f. of the asset return distribution at the end of the monitoring period:

$$\text{VaR}(\tau,\chi) = S_t - e^{\overline{\kappa}}, \quad \text{given that} \quad p(x,\tau;\overline{\kappa}) = 1-\chi. \tag{29}$$

Equations (26) and (29) can be solved using, e.g., the bisection method.

Finally, we note that it can be verified that

$$\text{VaR}(\tau,\chi) < \text{iVaR}(\tau,\chi), \quad \text{a.s. for} \quad \tau \in \mathbb{R}^+, \ \chi \in (0,1). \tag{30}$$

Intuitively, the probability of crossing a barrier level (from above) at any point in time during the monitoring period is higher than the probability that the underlying process will end up below the barrier level at the expiration date. Indeed the process which is in the stopping region at the end of the monitoring period has almost surely breached the barrier level before the expiration. Therefore, if a European and a one-touch digital put optionettes have identical prices, i.e., in our notation $p(x,\tau;\overline{\kappa}) = P(x,\tau;\underline{\kappa}) := 1-\chi$, then almost surely the implied barrier level $\underline{\kappa}$ (the iVaR) has to be lower (greater) than the implied strike $\overline{\kappa}$ (the VaR).

3.2 Pricing digital optionettes

We solve the PIDE system (24)–(25) using the Laplace-Carson transform (LCT) approach. For any locally integrable function $f : \mathbb{R}^+ \to \mathbb{R}$ and for all $\alpha \in \mathbb{R}^+$, the LCT is defined as

$$\left(\mathscr{LC}\right)_x [f(x)](\alpha) := \tilde{f}(\alpha) := \alpha \int_0^{+\infty} e^{-\alpha x} f(x) dx. \tag{31}$$

The main idea of our solution procedure is to compute the LCT of the optionette price with respect to the monitoring horizon τ. Applying the transformation to the PIDE (24) would eliminate the time dependence, hence effectively reducing the original pricing problem to an ordinary integro-differential equation (OIDE). Our results for European and one-touch digital put optionettes are summarized in Theorem 2 and Theorem 3, respectively.

The optionette prices in the time domain can be computed with the help of the Gaver-Stehfest inversion algorithm (GS) which reads as follows:

$$f_M(x) = \sum_{k=1}^{M} \varsigma_k \tilde{f}\left(\frac{k\log(2)}{x}\right), \tag{32}$$

where

$$\varsigma_k = \frac{(-1)^{M+k}}{k} \sum_{j=\lfloor (k+1)/2 \rfloor}^{\min\{k,M\}} \frac{j^{M+1}}{M!} \binom{M}{j} \binom{2j}{j} \binom{j}{k-j}. \tag{33}$$

It holds that

$$\lim_{M\to\infty} f_M(x) = f(x). \tag{34}$$

In expression (33), $\lfloor a \rfloor$ is defined as the greatest number $a' \in \mathbb{N}$ such that $a' \leq a$. It is important to point out that the Gaver-Stehfest algorithm takes place on the real line. Morever, the linear Salzer convergence acceleration scheme is included in the formula. We refer to Valkó and Abate (2004), Abate and Whitt (2006) and Kuznetsov (2013) for technical details about the GS inversion algorithm.

Laplace-Carson transforms of option price functions w.r.t. the time to maturity have the meaning of canadized options, e.g., see Carr (1998). We borrow this notation for the pricing digital optionettes, and derive our main theoretical results along the lines of Leippold and Vasiljević (2015), Theorem 1 and Theorem 2, pp. 7–8, 20–29.

Theorem 2 (**Canadized European digital put optionette**).
Assume that the asset price process $\{S_u, t \leq u \leq T\}$ *is described by the displaced mixed-exponential model (2). The price of a canadized European digital put optionette with the*

strike K and the monitoring horizon τ is thus given by

$$\tilde{p}(S_t,\alpha)=\begin{cases}1+\sum\limits_{i=1}^{\hat{m}}\underline{w}_i\left(\dfrac{S_t}{K}\right)^{\beta_{i,\alpha}} & \text{if } S_t<K,\\ \sum\limits_{j=1}^{\hat{n}}\overline{w}_j\left(\dfrac{S_t}{K}\right)^{\gamma_{j,\alpha}} & \text{if } S_t\geq K.\end{cases}\tag{35}$$

The coefficients $\{\beta_{i,\alpha}\}_{i=1,\ldots,\hat{m}}$, and $\{\gamma_{j,\alpha}\}_{j=1,\ldots,\hat{n}}$ are positive and negative roots of the characteristic equation $\Psi(u)=\alpha$, respectively, and the Lévy exponent $\Psi(\cdot)$ is defined in (5). The number of positive and negative characteristic roots depends on the LCT parameter α, i.e., it is equal to $\hat{m}:=\hat{m}(\alpha)\leq m+1$ and $\hat{n}:=\hat{n}(\alpha)\leq n+1$, respectively, where $\hat{m},\hat{n}\in\mathbb{N}$. The coefficients $\{\underline{w}_i\}_{i=1,\ldots,\hat{m}}$ and $\{\overline{w}_j\}_{j=1,\ldots,\hat{n}}$ can be computed by solving the system of linear equations

$$\mathbf{A}\mathbf{w}=\mathbf{a}.\tag{36}$$

The $(\hat{m}+\hat{n})$-dimensional column vector $\mathbf{w}$ and the $(m+n+2)$-dimensional column vector $\mathbf{a}$ are given in equations (69) and (70), respectively. The matrix $\mathbf{A}$ is an $(m+n+2)\times(\hat{m}+\hat{n})$-dimensional matrix given in equation (71).

Theorem 3 (**Canadized one-touch digital put optionette**).
Assume that the asset price process $\{S_u, t\leq u\leq T\}$ is described by the displaced mixed-exponential model (2). The price of a canadized one-touch digital put optionette with the barrier level K and the monitoring horizon τ is thus given by

$$\tilde{P}(S_t,\alpha)=\begin{cases}\sum\limits_{j=1}^{\hat{n}}v_j\left(\dfrac{S_t}{K}\right)^{\gamma_{j,\alpha}} & \text{if } S_t>K,\\ 1 & \text{if } S_t\leq K,\end{cases}\tag{37}$$

using the same notation as in Theorem 2. The set of coefficients $\{\overline{v}_j\}_{j=1,\ldots,\hat{n}}$ solve the system of linear equations

$$\mathbf{B}\mathbf{v}=\mathbf{b},\tag{38}$$

The $\hat{n}$-dimensional column vector $\mathbf{v}$ and the $(n+1)$-dimensional column vector $\mathbf{b}$ are given in equations (81) and (82), respectively. The matrix $\mathbf{B}$ is an $(n+1)\times\hat{n}$-dimensional

matrix given in equation (83).

3.3 First-passage disentanglement (FPD)

A one-touch digital put optionette is exercised if the asset price directly hits or overshoots the barrier at any point in time before maturity. Due to its almost sure continuity of paths, and conditionally on the stopping of the process, a Brownian motion almost surely hits the barrier separating the continuation from the stopping region; e.g., see Jeanblanc, Yor and Chesney (2009), Section 3, p. 135. On the other hand, an overshoot occurs if the asset price jumps over the barrier directly into the interior of the stopping region. More specifically, conditional on the stopping of the process due to a jump event, continuously distributed jumps almost surely induce an overshoot, i.e., the price process will almost surely not jump onto the barrier. Starting from the disentanglement results of Leippold and Vasiljević (2015), Theorem 3, pp. 9–10, 29–31, we show in Theorem 4 that precisely these properties allow us to quantify the first-passage disentanglement of the jump from the diffusion contribution to the stopping of the process, hence to the price of a one-touch digital put optionette and the iVaR value.

Theorem 4 (**Canadized first-passage disentanglement**).
Assume that the asset price process $\{S_u, t \leq u \leq T\}$ *is described by the displaced mixed-exponential model (2). The price of a canadized one-touch digital put optionette with the barrier level* K *and the monitoring horizon* τ *can be decomposed as*

$$\tilde{P}(S_t, \alpha) = \tilde{P}_D(S_t, \alpha) + \tilde{P}_J(S_t, \alpha). \tag{39}$$

The function $\tilde{P}_D(\cdot, \cdot)$ *represents the contribution of the diffusion process, i.e., the Brownian*

motion, which is given by

$$\tilde{P}_D(S_t, \alpha) = \begin{cases} \sum_{j=1}^{\hat{n}} \delta_j \left(\frac{S_t}{K}\right)^{\gamma_{j,\alpha}} & \text{if } S_t > K, \\ 1 & \text{if } S_t = K, \\ 0 & \text{if } S_t \leq K. \end{cases} \tag{40}$$

The function $\tilde{P}_J(\cdot, \cdot)$ *is the contribution of the jumps, i.e., the compound Poisson process, and it given by*

$$\tilde{P}_J(S_t, \alpha) = \begin{cases} \sum_{j=1}^{\hat{n}} \iota_j \left(\frac{S_t}{K}\right)^{\gamma_{j,\alpha}} & \text{if } S_t > K, \\ 0 & \text{if } S_t = K, \\ 1 & \text{if } S_t \leq K. \end{cases} \tag{41}$$

The sets of coefficients $\{\delta_j\}_{j=1,\ldots,\hat{n}}$ *and* $\{\iota_j\}_{j=1,\ldots,\hat{n}}$ *solve the systems of linear equations*

$$\begin{aligned} \mathbf{M}_D \boldsymbol{\delta} &= \boldsymbol{\epsilon}_D, \\ \mathbf{M}_J \boldsymbol{\iota} &= \boldsymbol{\epsilon}_J. \end{aligned} \tag{42}$$

The $\hat{n}$*-dimensional column vectors* $\boldsymbol{\delta}$ *and* $\boldsymbol{\iota}$ *are given in equations* (91) *and* (94)*, respectively. The* $(n+1)$*-dimensional column vectors* $\boldsymbol{\epsilon}_D$ *and* $\boldsymbol{\epsilon}_J$ *are given in equations* (92) *and* (95)*, respectively. The matrices* $\mathbf{M}_D$ *and* $\mathbf{M}_J$ *are identical* $(n+1) \times \hat{n}$*-dimensional matrices, which are equal to the matrix* $\mathbf{B}$ *defined for the one-touch digital put optionettes in equation* (83)*. The remaining notation is the same as in Theorem 2 and Theorem 3.*

4 Estimation of the jump models

The first step in our empirical investigation is the calibration of the jump models introduced in Section 2.3 under the physical and the risk-neutral measure. To achieve this goal, we use two different data sets: historical returns of the S&P 100 index and OEX American option quotes (bid and ask prices for different strikes and maturities). Additionally, we

use the zero-coupon curve data for the calibration under the risk-neutral measure.[17] All data used in our study is obtained from OptionMetrics.

Before the empirical findings are presented, we provide a rationale for our particular choice of option data. Generally, the most actively traded types of derivative contracts in financial markets are European and American options. We use American options because they are path-dependent, hence market quotes of American option prices embed the information about the set of events that might occur prior to the expiry. Therefore, due to the early exercise feature, market prices of American options reflect the first-passage probabilities and the intra-horizon risk. On the other hand, vanilla European options carry information only about the possible outcomes on a given future date, i.e., the maturity. Finally, it is well known that the pricing functional of an American-style option admits a decomposition into its European-style counterpart and the early exercise premium, which makes them informative about the end-of-horizon risk as well; e.g., see Detemple (2005) and references therein.

4.1 The data

Our first data set consists of 939 weekly historical returns of the S&P 100 index from January 1996 until August 2014, which are obtained by aggregating five successive daily return. It spans almost two decades and encompasses a broad spectrum of market conditions, including the recent global financial crisis. The data treatment for historical return time series follows closely Bakshi and Panayotov (2010), Section 5, pp. 25–26.[18] The ultimate goal of our study is to estimate 10-day VaR and iVaR levels; ideally, the sampling frequency that matches the monitoring horizon should be used. However, using the biweekly returns requires historical time series spanning very long periods of time.

[17] Similarly to Bakshi and Panayotov (2010), the dividends are neglected in our study. The reason is that the digital optionette approach for the computation of the VaR and the iVaR, which is introduced in Section 3, is valid only if the drift term of the underlying asset process (2) is equal to zero. This means that both the expected return and the dividend yield are assumed to be zero in the short term.

[18] Nevertheless, they investigate only the period 1995–2005 which does not include the most recent turbulent market conditions and the post-crisis period. On the other hand, our sample spans also the period 2005–2014. We believe that this is very important for our empirical study given that financial markets and the risk management practice have undergone a series of stupendous changes since 2008.

Even if the data were available, using observations from distant past might be misleading and irrelevant for the risk management. On the other hand, weekly returns are a better candidate than daily returns (which would exacerbate the frequency mismatch issue). Therefore, we compromise by using weekly historical return time series. Moreover, we follow the strategy to re-estimate models on monthly basis, and create moving/rolling windows of 260 weekly returns. This implies that first month for which we estimate the models will be January 2001 because we need 5 years of data to create a weekly time series of desired length.

The second data set used in our study contains option quotes exclusively. In particular, it is comprised of S&P 100 index American options data (ticker symbol: OEX), spanning the period from March 2001 until August 2014. The starting month of our option sample coincides with the first month for which we are able to estimate the models based on the time series of S&P 100 historical returns, conditional on the monthly re-calibration procedure and the choice of weekly sampling frequency. The last month in our sample for both data sets is determined by the availability of option quotes in the OptionMetrics database. Overall, this leaves us with 162 dates on which we estimate the models on both historical and option data. For re-calibration timestamps we choose those dates at the beginning of each month on which there exist liquid options maturing in exactly 10 trading days, hence matching the VaR/iVaR horizon.[19] Our procedure for selection of re-calibration dates introduces a subtle modification of Bakshi and Panayotov (2010) where options bear no weight whatsoever.

[Insert Table 1 about here]

Furthermore, for each date included the sample, the option data treatment is conducted as follows. We define moneyness m as the ratio of the strike K and the futures price $F_{t,T} := S_t e^{r(T-t)}$, i.e., $m := K/F_{t,T}$. In the first step, we eliminate all calls because by construction puts are much more informative of the downside risk in the underlying.[20]

[19] It turns out that most of the re-calibration dates chosen are first Mondays in each month. Sometimes re-calibration date is Tuesday or Wednesday if a national holiday happen to be on a Monday, e.g., the Independence Day or the Labor Day.

[20] For simplicity, we consider only the long position in the S&P 100 index, and therefore focus on the left tail of the distribution.

Second, we exclude illiquid in-the-money put options (ITM), i.e., puts with moneyness greater than 1.03. Hence, our sample contains only liquid near-the-money (NTM) and out-of-the-money (OTM) put options. To match the 10-day horizon (which is recommended by the regulators) for the computation of the risk measures, we keep only options with maturities equal or shorter than 10 days in our dataset. We use mid-prices, which are computed as averages of the bid and ask market quotes, as the proxy for our market prices. Option quotes lower than 0.125 units are eliminated due to the minimum tick limitations. Additionally, we eliminate the options with the zero volume or open interest. Descriptive statistics of our option sample are given in Table 1. The total number of option quotes in the dataset (spanning 162 days) is 3,411. NTM put options, i.e., options for which $m \in (0.97, 1.03)$, account for approximately 41.4 percent of the sample. OTM puts ($m < 0.97$) constitute around 58.6 percent of the dataset. The average implied volatility smile straddles the range from 21.15 percent (NTM puts) to 39.78 percent (OTM puts).

4.2 Calibration results

First, we estimate parameters for each of the considered models under the historical measure, which will serve as the benchmark in our empirical study. In particular, we conduct a rolling-window maximum likelihood estimation (MLE) using the weekly historical returns. However, there are two notable differences in our estimation approach from that of Bakshi and Panayotov (2010). Namely, we use the Fourier cosine method of Fang and Oosterlee (2008) to compute p.d.f. of the log-price process. Furthermore, we do not restrict the value of the fine structure parameter Y to 0.5 in the CGMY model. All values in the interval $Y \in (-1, 2)$ are allowed, which ensures an additional degree of freedom in the CGMY model. Second, the calibration under the risk-neutral measure is conducted by minimizing a loss function in the form of a weighted non-linear least squares (WNLLS) for each date in our sample. Our objective function can be interpreted as a weighted Euclidian distance between the market quotes and the corresponding model option prices, and the weights are defined as the inverses of squared bid-ask spreads.

[Insert Table 2 about here]

The most important statistics for both historical and option-based calibrations are summarized in Table 2. We report the average values and standard deviations of model parameters over the whole sample (162 days). Several patterns are observed across estimates. First, the option-implied estimates exhibit larger variation across time then the parameters estimated from the historical returns estimation. Arguably, this is due to better responsiveness of option-implied model parameters to the changing market conditions. However, the instability of the risk-neutral parameters could also be due to the non-convexity of the WNLLS loss function and the existence of multiple local minima; e.g., see Cont and Tankov (2004), Section 3.1, pp. 13–16. Second, for the infinite activity Lévy processes (FMLS, VG and CGMY), the jump arrival rate C is typically inversely proportional to the fine structure parameter Y. This is plausible because higher values of the fine structure parameter indicate increased activity of the small jumps, which are effectively "taking over" some part of the variation of the stochastic process (that would otherwise be captured by the jump intensity parameter). Third, the exponential decay parameters M and G are positively correlated with the parameter C. The reason is that the reciprocal values of M and G represent the average sizes of large jumps, which are inversely related to the jump intensity parameter due to the complete monotonicity. Forth, we observe across all models that average jump size is negative, hence indicating negative skewness.

4.3 Model performance

At first glance we observe similar performance for all models under the historical measure (MLE statistic in the Panel A of Table 2). The hierarchy among the four models is more apparent under the risk-neutral measure, e.g., CGMY model seems to provide the best fit to the option data (MSE statistic in the Panel B of Table 2). However, these values alone are not quite informative about model performance. To address this issue, we conduct Vuong (1989)'s closeness test (for non-nested models) for pairwise comparison of the

model calibration performance; see Table 3.

[Insert Table 3 about here]

Panel A summarizes the Vuong test statistics for the historical estimation. The calibration performance ordering among the models is: VG $\succ$ FMLS $\succ$ MJD $\succ$ CGMY. On the other hand, the hierarchy of the models looks different for the option-based estimation (Panel B): CGMY $\succ$ MJD $\succ$ VG $\succ$ FMLS.[21] We therefore conclude that the model performance rankings are inconsistent under the historical and the risk-neutral measure. This finding corroborates the argument that the informational content of the two measures is different, and it reinforces the importance of our research question regarding the relevance and the reliability of option-based estimates of risk measures—and more generally about the impact of the estimation risk—in the market risk management context.

5 Empirical results

5.1 VaR and iVaR estimates

To estimate VaR and iVaR we proceed as follows. First, we employ the approximation procedure outlined in Section 2.3, and obtain the historical and the risk-neutral D-MEM parameters corresponding to the calibrated Lévy models, i.e., MJD, FMLS, VG, and CGMY. Second, the risk-neutral parameters are translated into their risk-adjusted counterparts via the D-MEM change of measure derived in Section 2.2.

[Insert Figure 2 about here]

To demonstrate the outcome of the approximation concisely and instructively, the dynamics of the volatility parameter and the average jump size of the respective D-MEM approximations are presented in Figure 2. We plot the time series of the average volatility

[21] For two model (A and B) we write A $\succ$ B (B $\succ$ A) if the Vuong (1989)'s closeness test is rejected in favor of model A (B). We write A $\sim$ B if the test is not rejected.

and the average jump size with biweekly (10-day) horizon in view, which matches the regulatory monitoring period of of market risk measures.

Subsequently, using the D-MEM approximation results, the VaR and the iVaR estimates are computed—assuming 99.0% and 99.9% confidence levels, and 10-day monitoring horizon—via the digital optionette approach described in Section 3.1 and Section 3.2. Furthermore, for each observation date in the sample, we decompose the estimated iVaR into a diffusion and a jump component by applying the theoretical results for the first-passage disentanglement given in Section 3.3. The time evolution of the jump contribution to the iVaR (in the sense of Theorem 4) is presented in Figure 3. The results are striking: Irrespectively of the model and the estimation procedure, jumps typically account for more than 80% of the iVaR, with an average of about 90%. This means that, if the critical intra-horizon reserve capital level is breached at some point in time before the expiry of the monitoring period, it is most likely caused by a jump in the asset price process (which almost surely incurs an overshoot, i.e., the loss beyond the predetermined set-aside cash buffer).

[Insert Figure 3 about here]

In the next step, following the procedure presented in Bakshi and Panayotov (2010), we quantify the impact of jumps and intra-horizon risk by computing the ratios of our jump models' VaR and iVaR estimates to a benchmark VaR value.[22] The benchmark is defined as the $(1-\chi)$-quantile of the normal distribution $\mathcal{N}(\hat{\mu}, \hat{\sigma}^2)$, where χ is either 99.0% or 99.9%. The parameter $\hat{\mu} = 0$ is the drift, and the parameter $\hat{\sigma}$ is the standard deviation of the of the (demeaned) return process under the historical measure. Therefore, assuming the aforementioned confidence levels, the benchmark VaR is equal to $(2.32\hat{\sigma} - \hat{\mu})$ and $(3.09\hat{\sigma} - \hat{\mu})$, respectively. The second benchmark VaR is constructed using the filtered historical simulation (FHS) approach of Barone-Adesi, Giannopoulos and Vosper (1999) and Barone-Adesi, Engle and Mancini (2008).[23]

[22] Bakshi and Panayotov (2010) used the term 'multiple' for these ratios. We adopt their notation, however it should be noted that Boudoukh et al. (2004) and Rossello (2008) used the term 'inflation factor' instead.

[23] Our FHS exercise is based on an AR(1)-GARCH(1,1) model with leverage effect under the historical

Our findings are summarized in Table 4. Panel A comprises average, median, and maximum values of the VaR and the iVaR multiples based on the estimation under the historical measure. Compared to the findings of Bakshi and Panayotov (2010), we estimate similar or lower (similar or higher) VaR and iVaR multiples at 99.0% (99.9%) confidence level. Almost uniformly, CGMY (FMLS) model has the lowest (highest) VaR and iVaR multiples. This result is even stronger for the more stringent confidence level, i.e., the relative difference of the CGMY (FMLS) multiples w.r.t. the other two jump models is amplified. Elevated FMLS multiples can be explained by the fact that it is the only spectrally negative process, and the only one without exponentially dampened Lévy density, among the four considered jump models. Overall, at 99.0% (99.9%) confidence level, a historical VaR estimator and a historical iVaR estimator can increase the benchmark level by the factor 1.99 (3.43) and 2.16 (3.52), respectively. Using the alternative benchmark VaR, we obtain the same rankings among the models. However, the multiples are partially dampened; the maximum multiples are 1.24 (2.11) and 1.35 (2.17) at 99.0% (99.9%) confidence level for the respective risk measures.

[Insert Table 4 about here]

Panel B reports the same descriptive statistics based on the multiples estimated under the risk-adjusted measure. We immediately observe that all multiples statistics are uniformly and significantly higher in this case. In other words, they are more conservative and thus provide a better protection against adverse market moves. Moreover, the forward-looking multiples exhibit larger variation across models, which can be interpreted as the model risk. However, the stupendous difference between the multiples estimated under the two probability measures (especially for the maximum iVaR multiples at 99.9% confidence level) strongly indicates that the estimation risk is probably even more important. In terms of the rankings under the risk-adjusted measure, MJD (CGMY) model has the lowest (highest) VaR and iVaR multiples. Using the risk-adjusted VaR

measure; see Monfort and Pegoraro (2012), Section 4.4.1, p. 1683. The algorithm is explained in detail in Barone-Adesi, Giannopoulos and Vosper (1999), pp. 585–587. We note that the GARCH model is estimated using 5 years of daily returns, i.e., 1,300 observations, and the FHS distributions of the cumulative returns and the running minima over 10-day horizon (from which we compute the VaR and the iVaR, respectively) arise from 10,000 replications of the filtered historical returns simulation.

and iVaR estimators can increase the benchmark level by the factor 7.61 (9.96) and 8.12 (9.96), respectively, at 99.0% (99.9%) confidence level. We note that the alternative VaR benchmark model yields again the same rankings. The maximum multiples with respect to the FHS VaR are 4.55 (5.64) and 4.86 (5.63) at 99.0% (99.9%) confidence level under the historical and the risk-adjusted measure, respectively.

[Insert Figure 4 and Figure 5 about here]

To illustrate better the behavior of multiples, we plot the time evolution of each model's iVaR multiples under the historical and the risk-adjusted measure in Figure 4. The results are computed at 99.0% confidence level at 10-day monitoring horizon. In contrast to the analysis presented above, we use 10-day VaR estimates of each jump model for a given probability measure as the benchmark (instead of a quantile of a normal distribution or an FHS distribution) to compute the respective multiples. By construction, the "within-model" iVaR multiples are informative about the marginal contribution of the intra-horizon risk component to the iVaR; see equation (30). Our findings indicate that, under both probability measures, the iVaR exceeds the corresponding VaR estimate by 5–12% percent, with an average of about 7.5–8.0% (with a notable exception of the risk-adjusted MJD for which we obtain somewhat lower values). On the other hand, it can be easily verified that the iVaR of a normal distribution (with mean zero, and irrespectively of the standard deviation) exceeds the corresponding VaR level by 10.7%. Within the scope of their empirical study, Bakshi and Panayotov (2010), Section 6.4, pp. 29–30, report that the average marginal contribution of the intra-horizon component to iVaR multiple is larger than the benchmark number stated above. They conclude that jumps have a tendency to increase the marginal contribution of the intra-horizon risk to the iVaR. However, our empirical results are pointing to the opposite effect, i.e., the expectation of jumps (in addition to the diffusion risk) typically elevates both risk metrics, but the VaR estimates seem to receive a stronger boost. Moreover, our findings are robust to the choice of probability measure.

Finally, we plot in Figure 5 the dynamics of the ratio of risk-adjusted and historical

iVaR estimates for each of the jump models separately.[24] The risk-adjusted iVaR estimates are lower than their historical counterparts in the calm market periods, i.e., the ratio is lower than one. Conversely, the ratio sharply rises during the financial and economic crises, most notably during the Stock market downturn of 2002, the Global financial crisis of 2008–2009, the European debt crisis of 2009–2010, and the Stock market downturn of 2011. Therefore, the risk-adjusted iVaR is more sensitive and responsive to the market conditions, and it can be interpreted as a risk measure implied by the market sentiment. Indeed, this is a rather expected result given the forward-looking nature of the risk metrics estimated under the risk-adjusted measure.

In summary, based on the empirical findings presented in this section, we conclude that the risk-adjusted iVaR estimates—with average (maximum) multiples in the range 1.69–2.02 (6.82–8.12)—can only partially explain the Basel multipliers, which fall in the range between 3 and 4. However, the results summarized in Table 4 and Figure 5 indicate that the Basel multipliers are often exaggerated in calm periods, thus unnecessarily inflating the risk metrics. On the other hand, historical estimates are not properly capturing the market sentiment when a crisis suddenly occurs. Moreover, it seems that the Basel multipliers do not provide a completely adequate compensation for the risk underestimation anomaly of VaR/iVaR estimates computed under the historical measure. Therefore, the implicit recommendation of the risk-adjusted approach to market risk management is to either use option-based estimates (whenever available) in addition to historical returns data, or to swiftly adjust, i.e., amplify, the current levels of Basel multipliers during imminent market turmoil periods (which is the time when their effectiveness is most needed).

5.2 Backtesting

To evaluate VaR (iVaR) forecasting performance of our jump models under the two probability measures, we retrieve the realized 10-day cumulative return (minimum interim cumulative return) for every observation date in the sample. In Figure 6 we compare

[24] The ratio of risk-adjusted and historical iVaR estimates follows almost identical pattern, hence we omit it in Figure 5.

the VaR estimates under the historical and the risk-adjusted measure with the realized returns. Additionally, we include the times series of FHS VaR estimates. An analogous plot for the iVaR is presented in Figure 7. In both cases, only the confidence level of 99.0% is considered.[25]

[Insert Figure 6 and Figure 7 about here]

We observe VaR and iVaR violations across all models. However, the forecasting performance is markedly different under the two measures. In particular, under the historical measure, there are typically 6–7 VaR breaches and 8–11 iVaR breaches out of total number of 162 observations. On the other hand, under the risk-adjusted measure, there are either no violations at all or at most one violation of VaR and iVaR critical levels. Therefore, the risk-adjusted estimates are evidently giving better results in terms of percentage of failures (up to 0.6% only for VaR and iVaR) relative to the historical estimates (3.7–4.3% for VaR and 4.9–6.8% for iVaR). Furthermore, the number of VaR and iVaR violations is the same under the risk-adjusted measures, whereas the number of iVaR breaches is larger that the number of VaR breaches under the historical measure. These results imply that the historical approach is less effective in capturing the intra-horizon component of iVaR. Finally, we notice a clustering behavior of VaR and iVaR violations in the months following the outbreak of the Global financial crisis of 2008, i.e., from October 2008 until February 2009. This finding strongly suggests that the assumption of the independence of VaR/iVaR violations does not hold.

[Insert Table 5 about here]

To properly evaluate the model performance we consider a battery of standard statistical tests. In particular, we employ the backtesting procedures of Kupiec (1995), i.e., the Time Until First Failure test (TUFF) and the Proportion of Failures test (POF), which is also known as the Unconditional Coverage test (UC). Moreover, we include the Independence Coverage test (IC) and the Conditional Coverage test (CC) of Christoffersen (1998). The results are summarized in Table 5, and they reinforce our earlier conclusions.

[25] We do not consider 99.9% confidence level because we have only 162 observations in our sample, which is not enough to make statistical inference on such a high confidence level.

Irrespectively of the jump model, historical VaR models provide relatively poor risk forecasts, hence they are largely rejected by the standard statistical tests (Panel A). Their performance additionally worsens in the case of iVaR backtesting (Panel C). On the other hand, risk-adjusted approach to the estimation of VaR and iVaR yields much better results (Panel B and Panel D, respectively). None of the models estimated under the forward-looking measure is rejected at the conventional confidence levels of 95% and 99%.[26] Nevertheless, we observe somewhat better performance of MJD and CGMY models in comparison to VG and FMLS models. Despite the fact that our findings are strongly in favor of the risk-adjusted measure-based estimation procedure, it is important to recognize that our sample size is relatively small, and that a more comprehensive and statistically reliable study would require a larger set of VaR/iVaR estimates.

6 Conclusion

This paper studies the intra-horizon value at risk (iVaR), which was previously considered in Boudoukh et al. (2004), Rossello (2008), Bhattacharyya, Misra and Kodase (2009) and Bakshi and Panayotov (2010). To enhance our understanding of theoretical and empirical results regarding the iVaR, we also analyze the end-of-horizon value at risk (VaR), which has been the risk management industry standard for more than two decades. First, we contribute to the current literature by developing a theoretical framework for the computation of VaR and iVaR, which encompasses both finite- and infinite-activity jump models. Additionally, we derive a new result for the disentanglement of the contribution of jumps from diffusion to the iVaR. Second, we apply our theoretical results to several popular Lévy models in a comprehensive empirical study using historical return time series and short-term American put options on S&P 100 index from March 2001 until August 2014. Our findings indicate that option-implied VaR and iVaR estimates and significantly higher (lower) than their historical counterparts in times of crisis (during calm market periods). Indeed, the statistical backtesting procedures which are employed in the paper

[26] These levels are not to be confused with the VaR/iVaR confidence level, which is set to $\chi = 99.0\%$.

provide a strong evidence that option-based VaR and iVaR forecasts exhibit a superior forecasting performance. Moreover, the intra-horizon feature further exacerbates the problems inherent to the historical approach. Our conclusion that the option-implied risk estimates provide a better protection against future adverse market moves can be explained by their forward-looking nature, which ultimately renders their remarkable perceptiveness and responsiveness to financial markets conditions. Our results under the historical and the risk-adjusted measure are consistent only for the empirical disentanglement of the contribution of jumps from diffusion to the iVaR—we find that jumps are the main driver of the intra-horizon risk, accounting for about 90% on average. Overall, our empirical findings are much more sensitive to the choice of probability measure (i.e., the dataset) than the choice of the model. Therefore, within the scope of our study, the estimation risk surpasses the model risk in importance. For this reason, we conclude that the option-implied estimation of risk measures should not be neglected in practice whenever option data is available.

References

Abate, J., W. Whitt. 2006. A unified framework for numerically inverting Laplace transforms. *INFORMS Journal on Computing* **18** 408–421.

Acerbi, C., D. Tasche. 2002a. On the coherence of expected shortfall. *Journal of Banking & Finance* **26** 1487–1503.

Acerbi, C., D. Tasche. 2002b. Expected shortfall: A natural coherent alternative to value at risk. *Economic Notes* **26** 379–388.

AitSahlia, F., A. Runnemo. 2007. A canonical optimal stopping problem for American options under a double exponential jump-diffusion model. *Journal of Risk* **10** 85–100.

Albrecher, H., D. Kortschak, X. Zhou. 2012. Pricing of Parisian options for a jump-diffusion model with two-sided jumps. *Applied Mathematical Finance* **19** 97–129.

Artzner, P., F. Delbaen, J. M. Eber, D. Heath. 1999. Coherent measures of risk. *Mathematical Finance* **9** 203–228.

Asmussen, S., D. Madan, M. Pistorius. 2007. Pricing equity default swaps under an approximation to the CGMY Lévy model. *Journal of Computational Finance* **11** 79–93.

Bakshi, G., G. Panayotov. 2010. First-passage probability, jump models, and intra-horizon risk. *Journal of Financial Economics* **95** 20–40.

Barone-Adesi, G., K. Giannopoulos, L. Vosper. 1999. VaR without correlations for portfolios of derivative securities. *Journal of Futures Markets* **19** 583–602.

Barone-Adesi, G., R. F. Engle, L. Mancini. 2008. A GARCH option pricing model with filtered historical simulation. *Review of Financial Studies* **21** 1223–1258.

Bartholomew, D. J. 1969. Sufficient conditions for a mixture of exponentials to be a probability density function. *The Annals of Mathematical Statistics* **40** 2183–2188.

Bayraktar, E., H. Xing. 2009. Pricing American options for jump diffusions by iterating optimal stopping problems for diffusions. *Mathematical Methods of Operations Research* **70** 505–525.

Bayraktar, E., H. Xing. 2011. Pricing Asian options for jump diffusion. *Mathematical Finance* **21** 117–143.

Bhattacharyya, M., N. Misra, B. Kodase. 2009. MaxVaR for non-normal and heteroskedastic returns. *Quantitative Finance* **9** 925–935.

Botta, R. F., C. M. Harris. 1986. Approximation with generalized hyperexponential distributions: Weak convergence results. *Queueing Systems* **1** 169–190.

Boudoukh, J., M. Richardson, R. Stanton, R. F. Whitelaw. 2004. MaxVaR: Long-horizon value at risk in a mark-to-market environment. *Journal of Investment Management* **2** 1–6.

Boyarcheko, M., S. Boyarchenko. 2011. Double barrier options in regime-switching hyper-exponential jump-diffusion models. *International Journal of Theoretical and Applied Finance* **14** 1005–1043.

Boyarchenko, S. I., S. Z. Levendorskiĭ. 2000. Option pricing for Truncated Lévy processes. *International Journal of Theoretical and Applied Finance* **3** 549–552.

Breeden, D. T., R. H. Litzenberger. 1978. Prices of state-contingent claims implicit in option prices. *Journal of Business* **51** 621–651.

Cai, N. 2009. On first passage times of a hyper-exponential jump diffusion process. *Operations Research Letters* **37** 127–134.

Cai, N., N. Chen, X. Wan. 2009. Pricing double-barrier options under a flexible jump diffusion model. *Operations Research Letters* **37** 163–167.

Cai, N., N. Chen, X. Wan. 2010. Occupation times of jump-diffusion processes with double exponential jumps and the pricing of options. *Mathematics of Operations Reserach* **35** 412–437.

Cai, N. 2011. Pricing and hedging quantile options in a flexible jump diffusion model. *Journal of Applied Probability* **48** 637–656.

Cai, N., S. Kou. 2011. Option pricing under a mixed-exponential jump diffusion model. *Management Science* **57** 2067–2081.

Cai, N., S. Kou. 2012. Pricing Asian options under a hyper-exponential jump-diffusion model. *Operations Research* **60** 64–77.

Cai, N., L. Sun. 2014. Valuation of stock loans with jump risk. *Journal of Economic Dynamics & Control* **40** 213–241.

Carr, P. 1998. Randomization and the American put. *The Review of Financial Studies* **11** 597–626.

Carr, P., H. Geman, D. B. Madan, M. Yor. 2002. The fine structure of asset returns: An empirical investigation. *Journal of Business* **75** 305–332.

Carr, P., L. Wu. 2003. The finite moment log stable process and option pricing. *The Journal of Finance* **58** 753–778.

Carr, P., L. Wu. 2004. Time-changed Lévy processes and option pricing. *Journal of Financial Economics* **71** 113–141.

Chan, T. 1999. Pricing contingent claims on stocks driven by LÃ©vy processes. *Annals of Applied Probability* **9** 504–528.

Christoffersen, P., 1998. valuating interval forecasts. *International Economic Review* **39** 841–862.

Christoffersen, P., K. Jacobs, B. Y. Chang. 2013. Forecasting with option-implied information. *Handbook of Economic Forecasting* Vol. 2A 581–656. Elsevier.

Cont, R., P. Tankov. 2004. Non-parametric calibration of jump-diffusion option pricing models. *Journal of Computational Finance* **7** 1–50.

Crosby, J., N. Le Saux, A. Mijatović. 2010. Approximating Lévy processes with a view to option prices. *International Journal of Theoretical and Applied Finance* **13** 63–91.

Detemple, J. 2005. American-style derivatives: Valuation and computation. CRC Press.

Duffie, D., J. Pan. 1997. An overview of value at risk. *The Journal of Derivatives* **4** 7–49.

Eberlein, E., U. Keller. 1995. Hyperbolic distributions in finance. *Bernoulli* **1** 281–299.

Esscher, F. 1932. On the probability function in the collective theory of risk. *Skandinavisk Aktuarietidskrift* **15** 175–195.

Fabozzi, F. J., A. Leccadito, R. S. Tunaru. 2014. Extracting market information from equity

options with exponential Lévy processes. *Journal of Economic Dynamics & Control* **38** 125–141.

Fang, F., C. W. Oosterlee. 2008. A novel pricing method for European options based on Fourier-cosine series expansions. *SIAM Journal of Scientific Computating* **31** 826–848.

Fuh, C.-D., S.-F. Luo, J.-F. Yen. 2013. Pricing discrete path-dependent options under a double exponential jump-diffusion model. *Journal of Banking & Finance* **37** 2702–2713.

Gerber, H. U., E. S. W. Shiu. 1994. Option prices by Esscher transforms. *Transactions of Society of Actuaries* **46** 99–191.

Hackmann, D., A. Kuznetsov. 2014. Approximating Lévy processes with completely monotone jumps. arXiv preprint. arXiv:1404.0597.

Hofer, M., P. Mayer. 2013. Pricing and hedging of lookback options in hyper-exponential jump-diffusion model. *Applied Mathematical Finance* **20** 489–511.

Hubalek, F., C. Sgarra. 2006. Esscher transforms and the minimal entropy martingale measure for exponential Lévy models. *Quantitative Finance* **6** 125–145.

Jeanblanc, M., M. Yor, M. Chesney. 2009. Mathematical methods for financial markets. Springer.

Jeannin, M., M. Pistorius. 2010. A transform approach to compute prices and Greeks of barrier options driven by a class of Lévy processes. *Quantitative Finance* **10** 629–644.

Koponen, I. 1995. Analytic approach to the problem of convergence of truncated Lévy flights towards the Gaussian stochastic process. *Physical Review E* **52** 1197–1199.

Kou, S. G. 2002. A jump-diffusion model for option pricing. *Management Science* **48** 1086–1101.

Kou, S. G., H. Wang. 2003. First passage times of a jump diffusion process. *Advances in Applied Probability* **35** 504–531.

Kou, S. G., H. Wang. 2004. Option pricing under a double exponential jump diffusion model. *Management Science* **35** 1178–1192.

Kou, S. G., G. Petrella, H. Wang. 2005. Pricing path-dependent options with jump risk via Laplace transforms. *The Kyoto Economic Review* **74** 1–23.

Kritzman, M., D. Rich. 2002. The mismeasurement of risk. *Financial Analysts Journal* **58** 91–99.

Kupiec, P. H., 1995. Techniques for verifying the accuracy of risk measurement models. *The Journal of Derivatives* **3** 73–84.

Kuznetsov, A. 2013. On the convergence of the Gaver-Stehfest algorithm. *SIAM Journal of Numerical Analysis* **51** 2984–2998.

Latané, H. A., R. J. Rendleman. 1976. Standard deviations of stock price ratios implied in option prices. *The Journal of Finance* **31** 369–381.

Leippold, M., N. Vasiljević. 2015. Pricing and disentanglement of American puts in the hyper-exponential jump-diffusion model. Swiss Finance Institute Research Paper No. 15-08, http://papers.ssrn.com/sol3/papers.cfm?abstract_id=2571208.

Lipton, A. 2002. Assets with jumps. *Risk* **15** 149–153.

Madan, D. B., E. Seneta. 1990. The variance gamma (V.G.) model for share market returns. *Journal of Business* **63** 511–524.

Merton, R. C. 1976. Option pricing when underlying stock returns are discontinuous. *Journal of Financial Economics* **3** 125–144.

Milne, F., D. B. Madan. 1990. Option pricing with V.G. martingale components. *Mathematical Finance* **1** 39–55.

Miyahara, Y. 1999. Minimal entropy martingale measures of jump type price processes in incomplete assets markets. *Asia-Pacific Financial Markets* **6** 97–113.

Monfort, A., F. Pegoraro. 2012. Asset pricing with second-order Esscher transforms. *Journal of Banking & Finance* **36** 1678–1687.

Ramezani, C. A., Y. Zeng. 2007. Maximum likelihood estimation of the double exponential jump-diffusion process. *Annals of Finance* **3** 487–507.

Rockafellar, R. T., S. Uryasev. 2002. Conditional value-at-risk for general loss distributions. *Journal of Banking & Finance* **26** 1443–1471.

Rossello, D. 2008. MaxVaR with non-Gaussian distributed returns. *European Journal of Operational Research* **189** 159–171.

Sato, K.-I. 1999. *Lévy processes and infinitely divisible distributions*. Cambridge Studies in Advanced Mathematics Vol. 68 (Cambridge University Press).

Sepp, A. 2004. Analytical pricing of double-barrier options under a double-exponential jump diffusion process — Applications of Laplace transform. *International Journal of Theoretical and Applied Finance* **7** 151–175.

Steutel, F. W. 1967. Note on the infinite divisibility of exponential mixtures. *The Annals of Mathematical Statistics* **38** 1303–1305.

Stulz, R. 1996. Rethinking risk management. *Journal of Applied Corporate Finance* **9** 8–24.

Thul, M., A. Q. Zhang. 2014. Analytical option pricing under an asymmetrically displaced double

gamma jump-diffusion model. 26th Australasian Finance and Banking Conference 2013. http://papers.ssrn.com/sol3/papers.cfm?abstract_id=2311673.

Toivanen, J. 2008. Numerical valuation of European and American options under Kou's jump-diffusion model. *SIAM Journal of Scientific Computing* **30** 1949–1970.

Valkó, P. P., J. Abate. 2004. Comparison of sequence accelerators for the Gaver method of numerical Laplace transform inversion. *Computers and Mathematics with Applications* **48** 629–636.

Vuong, Q. H. 1989. Likelihood ratio tests for model selection and non-nested hypotheses. *Econometrica* **57** 307–333.

Wong, H. Y., K. Y. Lau. 2013. Analytical valuation of turbo warrants under double exponential jump diffusion. *The Journal of Derivatives* **9** 61–73.

Wu, L. 2006. Dampened power law: Reconciling the tail behavior of financial security returns. *The Journal of Business* **79** 1445–1473.

Yin, C., Y. Shen, Y. Wen. 2013. Exit problems for jump processes with applications to dividend problems. *Journal of Computational and Applied Mathematics* **245** 30–52.

Appendix A The change of measure

A.1 Proof of Theorem 1: Risk-neutral dynamics

The Esscher transform of D-MEM process is

$$Z_t(\vartheta) := \left.\frac{d\mathbb{Q}^\vartheta}{d\mathbb{P}}\right|_{\mathcal{F}_t} = \underbrace{e^{\vartheta\sigma W_t - \frac{1}{2}\vartheta^2\sigma^2 t}}_{Z_t^D(\vartheta)} \underbrace{e^{\vartheta\sum_{i=1}^{N_t} Y_i - t\Psi_J(\vartheta)}}_{Z_t^J(\vartheta)}. \tag{43}$$

First, it follows from the Girsanov theorem that the $\mathbb{Q}^\vartheta$-Brownian motion is $W_t^* = W_t - [W, \vartheta\sigma W]_t = W_t - \vartheta\sigma t$. The volatility parameter remains the same after the change of measure, i.e., $\sigma^* = \sigma$. Second, it can be shown that the cumulant generating function (c.g.f.) of the jump part is given by

$$\Psi_J(a) = \lambda\left(\left(\frac{\lambda_+}{\lambda}\sum_{i=1}^{m}\frac{p_i\eta_i}{\eta_i - a} + \frac{\lambda_-}{\lambda}\sum_{j=1}^{n}\frac{q_j\theta_j}{\theta_j + a}\right)e^{a\xi}\right) - 1, \tag{44}$$

for every $a \in (-\theta_1, \eta_1)$. The jump c.g.f. under the new measure is

$$\Psi_J^*(\varkappa) := \frac{1}{t}\log\mathbb{E}\left[Z_t^J(\vartheta)e^{\varkappa\sum_{i=1}^{N_t} Y_i}\right] = \Psi_J(\varkappa + \vartheta) - \Psi_J(\vartheta), \tag{45}$$

for every $\varkappa \in (-\theta_1, \eta_1)$. This equation can be written in the form

$$\begin{aligned}\Psi_J^*(\varkappa) &= \lambda\int_{-\infty}^{+\infty}(e^{\varkappa y} - 1)\, e^{\vartheta y} f_Y(y)dy \\ &= \lambda^*\int_{-\infty}^{+\infty}(e^{\varkappa y} - 1)\,\frac{e^{\vartheta y} f_Y(y)}{\int_{-\infty}^{+\infty} e^{\vartheta y} f_Y(y)dy}dy,\end{aligned} \tag{46}$$

where the jump intensity under the new measure is given by

$$\lambda^* := \lambda\int_{-\infty}^{+\infty} e^{\vartheta y} f_Y(y)dy = \underbrace{\lambda_+\sum_{i=1}^{m}\frac{p_i\eta_i}{\eta_i - \vartheta}e^{\vartheta\xi}}_{\lambda_+^*} + \underbrace{\lambda_-\sum_{j=1}^{n}\frac{q_j\theta_j}{\theta_j + \vartheta}e^{\vartheta\xi}}_{\lambda_-^*}, \tag{47}$$

and the exponentially tilted jump size distribution under the new measure is defined as

$$f_Y^*(y) := \frac{e^{\vartheta y} f_Y(y)}{\int_{-\infty}^{+\infty} e^{\vartheta y} f_Y(y) dy}. \tag{48}$$

After some algebraic calculation, we obtain the expression for the jump c.g.f. under risk-neutral measure

$$\Psi_J^*(\varkappa) = \lambda^* \left(\left(\frac{\lambda_+^*}{\lambda^*} \sum_{i=1}^{m} \frac{p_i^* \eta_i^*}{\eta_i^* - \varkappa} + \frac{\lambda_-^*}{\lambda^*} \sum_{j=1}^{n} \frac{q_j^* \theta_j^*}{\theta_j^* + \varkappa} \right) e^{\varkappa \xi^*} \right) - 1. \tag{49}$$

The coefficients λ_+^* and λ_-^* are defined in equation (47). Furthermore, for all $i = 1, 2, ..., m$ we have that $\eta_i^* = \eta_i - \vartheta$ and $p_i^* = p_i \frac{\eta_i}{\eta_i - \vartheta} \frac{1}{\upsilon_+(\vartheta)}$, and for all $j = 1, 2, ..., n$ the adjusted coefficients are $\theta_j^* = \theta_j + \vartheta$ and $q_j^* = q_j \frac{\theta_j}{\theta_j + \vartheta} \frac{1}{\upsilon_-(\vartheta)}$. The introduced υ-coefficients are: $\upsilon_+(\vartheta) = \sum_{i=1}^{m} \frac{p_i \eta_i}{\eta_i - \vartheta}$ and $\upsilon_-(\vartheta) = \sum_{j=1}^{n} \frac{q_j \theta_j}{\theta_j + \vartheta}$. The displacement parameter ξ remain unchanged, i.e., $\xi^* = \xi$. Thus, we conclude that the log-price process under the measure $\mathbb{Q}^\vartheta$ is described by (9).

It remains to find the value of the Esscher transform parameter ϑ which guarantees that the new probability measure is indeed the risk-neutral measure. We require that the discounted process $\left\{ e^{-rt} S_t, t \geq 0 \right\}$ is a $\mathbb{Q}^\vartheta$-martingale, i.e.,

$$\mathbb{E}^* \left[e^{-rt + X_t} \right] = e^{(\bar{\mu} - r)t} \mathbb{E} \left[Z_t(\vartheta) e^{\frac{1}{2}(2\omega + 1)\sigma^2 t} e^{(\Psi_J(\vartheta + 1) - \Psi_J(\vartheta))t} \right] = 1. \tag{50}$$

Therefore, our equivalent martingale measure $\mathbb{Q}^\vartheta$ is indeed the risk-neutral measure if the Esscher transform parameter solves computed the equation

$$\bar{\mu} - r + \left(\vartheta + \frac{1}{2} \right) \sigma^2 + \Psi_J(\vartheta + 1) - \Psi_J(\vartheta) = 0. \tag{51}$$

It can be easily verified that this equation can be reduced to the form (11). This The proof of existence and uniqueness of ϑ for the change of measure via Esscher transform is given in Thul and Zhang (2014), Proposition 2, pp. 12–13. ■

Appendix B Digital optionette approach

B.1 Proof of Theorem 2: Pricing of canadized European digital put optionettes in D-MEM framework

Taking the Laplace-Carson transform (LCT) of the PIDE system for European digital put optionette, we obtain the ordinary integro-differential equation (OIDE) for the canadized European put optionette $\tilde{p} := \tilde{p}(x,\alpha)$:

$$\frac{\sigma^2}{2}\frac{d^2\tilde{p}}{dx^2}(x,\alpha)+\bar{\varrho}\frac{d\tilde{p}}{dx}(x,\alpha)-(\lambda+\alpha)\tilde{p}(x,\alpha)+\alpha\mathbb{1}_{\{x<\kappa\}}+\lambda\int_{-\infty}^{+\infty}\tilde{p}(x+y,\alpha)f_Y(y)dy=0, \quad (52)$$

where

$$f_Y(y)=\frac{\lambda_+}{\lambda}\sum_{i=1}^{m}p_i\eta_i e^{-\eta_i(y-\xi)}\mathbb{1}_{\{y\geq\xi\}}+\frac{\lambda_-}{\lambda}\sum_{j=1}^{n}q_j\theta_j e^{\theta_j(y-\xi)}\mathbb{1}_{\{y<\xi\}}. \quad (53)$$

The boundary conditions are

$$\begin{aligned}\lim_{x\downarrow-\infty}\tilde{p}(x,\alpha)&=1,\\ \lim_{x\uparrow+\infty}\tilde{p}(x,\alpha)&=0.\end{aligned} \quad (54)$$

The initial condition, which is given by the third equation in (25), is absorbed in the equation (52) due to the LCT. We conjecture the solution in the form

$$\tilde{p}(x,\alpha)=\begin{cases}1+\sum_{l=1}^{\hat{m}}\underline{w}_l e^{\beta_{l,\alpha}(x-\kappa)} & \text{if } x<\kappa,\\ \sum_{l=1}^{\hat{n}}\overline{w}_l e^{\gamma_{l,\alpha}(x-\kappa)} & \text{if } x\geq\kappa.\end{cases} \quad (55)$$

The coefficients $\{\underline{w}_i\}_{i=1,\ldots,\hat{m}}$ and $\{\overline{w}_j\}_{j=1,\ldots,\hat{n}}$ can be calculated by analyzing the solution in the two different regions, i.e., below and above the strike price, respectively.

First, we consider the case $x<\kappa$. It is straightforward to compute the two derivative

terms in (52), i.e.,

$$\begin{aligned}\frac{d\tilde{p}}{dx}(x,\alpha) &= \sum_{l=1}^{\hat{m}} \underline{w}_l \beta_{l,\alpha} e^{\beta_{l,\alpha}(x-\kappa)},\\ \frac{d^2\tilde{p}}{dx^2}(x,\alpha) &= \sum_{l=1}^{\hat{n}} \underline{w}_l \beta_{l,\alpha}^2 e^{\beta_{l,\alpha}(x-\kappa)}.\end{aligned} \tag{56}$$

On the other hand, the integral term is much more involved. We introduce the change of variables $y' := y - \xi$, which transforms the jump distribution:

$$f_{Y'}(y') = \frac{\lambda_+}{\lambda} \sum_{i=1}^{m} p_i \eta_i e^{-\eta_i y'} \mathbb{1}_{\{y' \geq 0\}} + \frac{\lambda_-}{\lambda} \sum_{j=1}^{n} q_j \theta_j e^{\theta_j y'} \mathbb{1}_{\{y' < 0\}}. \tag{57}$$

Consequently, the integral in the equation (52) becomes

$$\mathscr{I} := \int_{-\infty}^{+\infty} \tilde{p}(x+y,\alpha) f_Y(y) dy = \int_{-\infty}^{+\infty} \tilde{p}(x+\xi+y',\alpha) f_Y(y') dy'. \tag{58}$$

It can further be decomposed as

$$\begin{aligned}\mathscr{I} = &\frac{\lambda^-}{\lambda} \sum_{l=1}^{\hat{m}} \sum_{j=1}^{n} \int_{-\infty}^{0} q_j \theta_j \underline{w}_l e^{\beta_{l,\alpha}(x+\xi-\kappa)} e^{(\beta_{l,\alpha}+\theta_j)y'} dy'\\ &+ \frac{\lambda^-}{\lambda} \sum_{j=1}^{n} \int_{-\infty}^{0} q_j \theta_j e^{\theta_j y'} dy'\\ &+ \frac{\lambda^+}{\lambda} \sum_{l=1}^{\hat{m}} \sum_{i=1}^{m} \int_{0}^{\kappa-x} p_i \eta_i \underline{w}_l e^{\beta_{l,\alpha}(x+\xi-\kappa)} e^{(\beta_{l,\alpha}-\eta_i)y'} dy'\\ &+ \frac{\lambda^+}{\lambda} \sum_{l=1}^{m} \int_{0}^{\kappa-x} p_l \eta_l e^{-\eta_l y'} dy'\\ &+ \frac{\lambda^+}{\lambda} \sum_{i=1}^{m} \sum_{l=1}^{\hat{n}} \int_{\kappa-x}^{+\infty} p_i \eta_i \overline{w}_l e^{\gamma_{l,\alpha}(x+\xi-\kappa)} e^{(\gamma_{l,\alpha}-\eta_i)y'} dy'.\end{aligned} \tag{59}$$

After some algebra, the OIDE (52) yields the following condition

$$\sum_{l=1}^{\hat{m}} \underline{w}_l e^{\beta_{l,\alpha}(x-\kappa)} \left(\Psi(\beta_{l,\alpha}) - \alpha\right) - \sum_{l=1}^{m} \lambda^+ \eta_l e^{\eta_l(x-\kappa)} \left(\sum_{i=1}^{\hat{m}} \frac{\underline{w}_i e^{\beta_{i,\alpha}\xi}}{\eta_l - \beta_{i,\alpha}} - \sum_{j=1}^{\hat{n}} \frac{\overline{w}_j e^{\gamma_{j,\alpha}\xi}}{\eta_l - \gamma_{j,\alpha}} + \frac{1}{\eta_l} \right) = 0, \tag{60}$$

for all $l = 1, 2, ..., m$. Using the definition of the cumulant generating function (5) and the characteristic equation (6), we conclude that the first sum in (60) is equal to zero. Therefore, we obtain a system of m linear equations for the coefficients $\{\underline{w}_i\}_{i=1,...,\hat{m}}$ and $\{\overline{w}_j\}_{j=1,...,\hat{n}}$, i.e.,

$$\sum_{i=1}^{\hat{m}} \frac{\underline{w}_i e^{\beta_{i,\alpha}\xi}}{\eta_l - \beta_{i,\alpha}} - \sum_{j=1}^{\hat{n}} \frac{\overline{w}_j e^{\gamma_{j,\alpha}\xi}}{\eta_l - \gamma_{j,\alpha}} = -\frac{1}{\eta_l}, \quad \text{for } l = 1, ..., \hat{m}. \tag{61}$$

Now we study the case $x \geq \kappa$. First, the derivative terms are given by

$$\begin{aligned} \frac{d\tilde{p}}{dx}(x,\alpha) &= \sum_{l=1}^{\hat{n}} \overline{w}_l \gamma_{l,\alpha} e^{\gamma_{l,\alpha}(x-\kappa)}, \\ \frac{d^2\tilde{p}}{dx^2}(x,\alpha) &= \sum_{l=1}^{\hat{n}} \overline{w}_l \gamma_{l,\alpha}^2 e^{\gamma_{l,\alpha}(x-\kappa)}. \end{aligned} \tag{62}$$

The integral term can be decomposed as

$$\begin{aligned} \mathscr{I} = &\frac{\lambda^+}{\lambda} \sum_{l=1}^{\hat{n}} \sum_{i=1}^{m} \int_0^{+\infty} p_i \eta_i \overline{w}_l e^{\gamma_{l,\alpha}(x+\xi-\kappa)} e^{(\gamma_{l,\alpha}-\eta_i)y'} dy' \\ &+ \frac{\lambda^-}{\lambda} \sum_{j=1}^{n} \int_{-\infty}^{\kappa-x} q_j \theta_j e^{\theta_j y'} dy' \\ &+ \frac{\lambda^-}{\lambda} \sum_{l=1}^{\hat{n}} \sum_{j=1}^{n} \int_{\kappa-x}^{0} q_j \theta_j \overline{w}_l e^{\gamma_{l,\alpha}(x+\xi-\kappa)} e^{(\gamma_{l,\alpha}+\theta_j)y'} dy' \\ &+ \frac{\lambda^-}{\lambda} \sum_{j=1}^{n} \sum_{l=1}^{\hat{m}} \int_{-\infty}^{\kappa-x} q_j \theta_j \underline{w}_l e^{\beta_{l,\alpha}(x+\xi-\kappa)} e^{(\beta_{l,\alpha}+\theta_j)y'} dy'. \end{aligned} \tag{63}$$

Again, after some lengthy calculations we obtain the condition

$$\sum_{l=1}^{\hat{n}} \overline{w}_l e^{\gamma_{l,\alpha}(x-\kappa)} \left(\Psi(\gamma_{l,\alpha}) - \alpha\right) + \sum_{l=1}^{n} \lambda^- q_l \theta_l e^{\theta_l(x-\kappa)} \left(\sum_{i=1}^{\hat{m}} \frac{\underline{w}_i e^{\beta_{i,\alpha}\xi}}{\theta_l + \beta_{i,\alpha}} - \sum_{j=1}^{\hat{n}} \frac{\overline{w}_j e^{\gamma_{j,\alpha}\xi}}{\theta_l + \gamma_{j,\alpha}} + \frac{1}{\theta_l} \right) = 0. \tag{64}$$

Using the same arguments as in the case $x < \kappa$, we get the following set of conditions:

$$\sum_{i=1}^{\hat{m}} \frac{\underline{w}_i e^{\beta_{i,\alpha}\xi}}{\theta_l + \beta_{i,\alpha}} - \sum_{j=1}^{\hat{n}} \frac{\overline{w}_j e^{\gamma_{j,\alpha}\xi}}{\theta_l + \gamma_{j,\alpha}} = -\frac{1}{\theta_l}, \quad \text{for } l = 1, ..., \hat{n}. \tag{65}$$

To close the system of equations we use the value matching and the smooth pasting conditions at $x = \kappa$:

$$\begin{aligned} \lim_{x\uparrow\kappa} \tilde{p}(x,\alpha) &= \lim_{x\downarrow\kappa} \tilde{p}(x,\alpha), \\ \lim_{x\uparrow\kappa} \frac{d\tilde{p}}{dx}(x,\alpha) &= \lim_{x\downarrow\kappa} \frac{d\tilde{p}}{dx}(x,\alpha). \end{aligned} \tag{66}$$

Therefore, we have

$$\begin{aligned} \sum_{i=1}^{\hat{m}} \underline{w}_i - \sum_{j=1}^{\hat{n}} \overline{w}_j &= -1, \\ \sum_{i=1}^{\hat{m}} \beta_{i,\alpha} \underline{w}_i - \sum_{j=1}^{\hat{n}} \gamma_{j,\alpha} \overline{w}_j &= 0. \end{aligned} \tag{67}$$

After collecting the conditions (61), (65), and (67) we obtain the following system of linear equations:

$$\mathbf{A}\mathbf{w} = \mathbf{a}, \tag{68}$$

where

$$\mathbf{w} := (\underline{w}_1, ..., \underline{w}_{\hat{m}}, \overline{w}_1, ..., \overline{w}_{\hat{n}})' \tag{69}$$

is an $(\hat{n} + \hat{m})$-dimensional column vector, and

$$\mathbf{a} := \left(-1, 0, -\frac{1}{\eta_1}, ..., -\frac{1}{\eta_m}, -\frac{1}{\theta_1}, ..., -\frac{1}{\theta_n}\right)' \tag{70}$$

is an $(m+n+2)$-dimensional column vectors. Lastly, the matrix $\mathbf{A}$ is defined as

$$\mathbf{A} := \begin{pmatrix} 1 & \cdots & 1 & -1 & \cdots & -1 \\ \beta_{1,\alpha} & \cdots & \beta_{\hat{m},\alpha} & -\gamma_{1,\alpha} & \cdots & -\gamma_{\hat{n},\alpha} \\ \frac{e^{\beta_{1,\alpha}\xi}}{\eta_1-\beta_{1,\alpha}} & \cdots & \frac{e^{\beta_{\hat{m},\alpha}\xi}}{\eta_1-\beta_{\hat{m},\alpha}} & -\frac{e^{\gamma_{1,\alpha}\xi}}{\eta_1-\gamma_{1,\alpha}} & \cdots & -\frac{e^{\gamma_{\hat{n},\alpha}\xi}}{\eta_1-\gamma_{\hat{n},\alpha}} \\ \vdots & \ddots & \vdots & \vdots & \ddots & \vdots \\ \frac{e^{\beta_{1,\alpha}\xi}}{\eta_m-\beta_{1,\alpha}} & \cdots & \frac{e^{\beta_{\hat{m},\alpha}\xi}}{\eta_m-\beta_{\hat{m},\alpha}} & -\frac{e^{\gamma_{1,\alpha}\xi}}{\eta_m-\gamma_{1,\alpha}} & \cdots & -\frac{e^{\gamma_{\hat{n},\alpha}\xi}}{\eta_m-\gamma_{\hat{n},\alpha}} \\ \frac{e^{\beta_{1,\alpha}\xi}}{\theta_1+\beta_{1,\alpha}} & \cdots & \frac{e^{\beta_{\hat{m},\alpha}\xi}}{\theta_1+\beta_{\hat{m},\alpha}} & -\frac{e^{\gamma_{1,\alpha}\xi}}{\theta_1+\gamma_{1,\alpha}} & \cdots & -\frac{e^{\gamma_{\hat{n},\alpha}\xi}}{\theta_1+\gamma_{\hat{n},\alpha}} \\ \vdots & \ddots & \vdots & \vdots & \ddots & \vdots \\ \frac{e^{\beta_{1,\alpha}\xi}}{\theta_n+\beta_{1,\alpha}} & \cdots & \frac{e^{\beta_{\hat{m},\alpha}\xi}}{\theta_n+\beta_{\hat{m},\alpha}} & -\frac{e^{\gamma_{1,\alpha}\xi}}{\theta_n+\gamma_{1,\alpha}} & \cdots & -\frac{e^{\gamma_{\hat{n},\alpha}\xi}}{\theta_n+\gamma_{\hat{n},\alpha}} \end{pmatrix}. \tag{71}$$

This concludes the proof. ■

B.2 Proof of Theorem 3: Pricing of canadized one-touch digital put optionettes in D-MEM framework

The proof is similar to the one provided for canadized European digital put optionettes. A notable difference is that we have two different regions in the case of one-touch digital put optionettes: the continuation region ($x > \kappa$) and the stopping region ($x \leq \kappa$). The Laplace-Carson transform of the PIDE system for one-touch digital put optionette (24)–(25) yields the following OIDE in the continuation region

$$\frac{\sigma^2}{2}\frac{d^2\tilde{P}}{dx^2}(x,\alpha) + \bar{\varrho}\frac{d\tilde{P}}{dx}(x,\alpha) - (\lambda+\alpha)\tilde{P}(x,\alpha) + \lambda\int_{-\infty}^{+\infty}\tilde{P}(x+y,\alpha)f_Y(y)dy = 0, \tag{72}$$

with the boundary conditions

$$\begin{aligned} \lim_{x\downarrow\kappa}\tilde{P}(x,\alpha) &= 1, \\ \lim_{x\uparrow+\infty}\tilde{P}(x,\alpha) &= 0. \end{aligned} \tag{73}$$

The initial condition is again absorbed in the resulting OIDE. We introduce the ansatz

$$\tilde{P}(x,\alpha) = \begin{cases} 1 & \text{if } \ x \leq \kappa, \\ \sum_{l=1}^{\hat{n}} v_l e^{\gamma_{l,\alpha}(x-\kappa)} & \text{if } \ x > \kappa. \end{cases} \tag{74}$$

W show below that the coefficients $\{v_j\}_{j=1,\ldots,\hat{n}}$ solve a system of linear equations.

The two derivative terms in (72) are

$$\begin{aligned} \frac{d\tilde{P}}{dx}(x,\alpha) &= \sum_{l=1}^{\hat{n}} v_l \gamma_{l,\alpha} e^{\gamma_{l,\alpha}(x-\kappa)}, \\ \frac{d^2\tilde{P}}{dx^2}(x,\alpha) &= \sum_{l=1}^{\hat{n}} v_l \gamma_{l,\alpha}^2 e^{\gamma_{l,\alpha}(x-\kappa)}. \end{aligned} \tag{75}$$

After applying the same change of jump size variable that is applied in the proof for European digital put optionettes, the integral term in equation (72) becomes

$$\begin{aligned} \mathscr{J} :&= \int_{-\infty}^{+\infty} \tilde{P}(x+\xi+y',\alpha) f_Y(y') dy' \\ &= \frac{\lambda^+}{\lambda} \sum_{l=1}^{\hat{n}} \sum_{i=1}^{m} \int_0^{+\infty} p_i \eta_i v_l e^{\gamma_{l,\alpha}(x+\xi-\kappa)} e^{(\gamma_{l,\alpha}-\eta_i)y'} dy' \\ &+ \frac{\lambda^-}{\lambda} \sum_{j=1}^{n} \int_{-\infty}^{\kappa-x} q_j \theta_j e^{\theta_j y'} dy' \\ &+ \frac{\lambda^-}{\lambda} \sum_{l=1}^{\hat{n}} \sum_{j=1}^{n} \int_{\kappa-x}^{0} q_j \theta_j v_l e^{\gamma_{l,\alpha}(x+\xi-\kappa)} e^{(\gamma_{l,\alpha}+\theta_j)y'} dy'. \end{aligned} \tag{76}$$

Solving the integrals on the r.h.s. gives us the condition

$$\sum_{l=1}^{\hat{n}} v_l e^{\gamma_{l,\alpha}(x-\kappa)} \left(\Psi(\gamma_{l,\alpha}) - \alpha\right) - \sum_{l=1}^{n} \lambda^- q_l \theta_l e^{\theta_l(\kappa-x)} \left(\sum_{j=1}^{\hat{n}} \frac{v_j e^{\gamma_{j,\alpha}\xi}}{\theta_l + \gamma_{j,\alpha}} - \frac{1}{\theta_l} \right) = 0. \tag{77}$$

Following the same logic as in the previous proof, the following n linear conditions emerge:

$$\sum_{j=1}^{\hat{n}} \frac{v_j e^{\gamma_{j,\alpha}\xi}}{\theta_l + \gamma_{j,\alpha}} = \frac{1}{\theta_l}, \quad \text{for } l = 1, \ldots, n. \tag{78}$$

We close the system with the value matching condition at the boundary between the exercise and the continuation region, which reads

$$\sum_{j=1}^{\hat{n}} v_j = 1. \tag{79}$$

Finally, we collect the conditions (78) and (79), and obtain the matrix equation

$$\mathbf{B}\mathbf{v} = \mathbf{b}, \tag{80}$$

where

$$\mathbf{v} := (v_1, v_2, ..., v_{\hat{n}})' \tag{81}$$

is $\hat{n}$-dimensional column vector, and

$$\mathbf{b} := \left(1, \frac{1}{\theta_1}, ..., \frac{1}{\theta_n}\right)' \tag{82}$$

is $(n+1)$-dimensional column vectors. Finally, the matrix $\mathbf{B}$ is $(n+1) \times \hat{n}$-dimensional matrix which is given by

$$\mathbf{B} := \begin{pmatrix} 1 & \cdots & 1 \\ \frac{e^{\gamma_{1,\alpha}\xi}}{\theta_1+\gamma_{1,\alpha}} & \cdots & \frac{e^{\gamma_{\hat{n},\alpha}\xi}}{\theta_1+\gamma_{\hat{n},\alpha}} \\ \vdots & \ddots & \vdots \\ \frac{e^{\gamma_{1,\alpha}\xi}}{\theta_n+\gamma_{1,\alpha}} & \cdots & \frac{e^{\gamma_{\hat{n},\alpha}\xi}}{\theta_n+\gamma_{\hat{n},\alpha}} \end{pmatrix}. \tag{83}$$

This completes the proof. ■

B.3 Proof of Theorem 4: First-passage disentanglement of canadized one-touch digital put optionettes in D-MEM framework

We showed in Theorem 3 that a canadized one-touch digital put optionette solves the OIDE (72) with the boundary conditions (73). It follows from the Feynman-Kac formula

that we can express the price of a canadized one-touch digital put optionette as

$$\tilde{P}(x,\alpha) = \mathbb{E}^x\left[e^{-\alpha(\tau_\kappa - t)}\right], \tag{84}$$

where τ_κ is the first-passage time (from above) of the barrier level κ for the log-price process X_t:

$$\tau_\kappa := \inf\{u \geq t : X_u \leq \kappa\}. \tag{85}$$

Mathematical formalism of the relationship between the OIDE system (72)–(73) and the expectation (85) can be derived by closely following the proof of Theorem 3.1 in Kou and Wang (2003), pp. 509–512, and Theorem 3.3 in Cai and Kou (2011), p. 2072. Since we are studying the Laplace transform of the first-passage time to a lower boundary, and the aforementioned papers study the Laplace transform of the first-passage time to an upper boundary, the formal proof is omitted in our paper.

Following the notation in Theorem 3 in Leippold and Vasiljević (2015), pp. 9–10, 29–31, the set $\mathscr{E}_{\mathcal{D}} := \{X_{\tau_\kappa} = \kappa\}$ represents all the possible events of the stopping of the process X_t exactly at the barrier κ, i.e., the stopping due to the diffusion. Similarly, we denote by $\mathscr{E}_{\mathcal{J}} := \{X_{\tau_\kappa} < \kappa\}$ the set of all possible events of the stopping due to overshooting of the barrier level κ by the process X_t, i.e., the stopping due to the jumps. The price of the canadized one-touch digital put optionette given in equation (84) can be orthogonally decomposed as

$$\tilde{P}(x,\alpha) = \mathbb{E}^x\left[e^{-\alpha(\tau_\kappa - t)}\mathbb{1}_{\mathscr{E}_{\mathcal{D}}}\right] + \sum_{j=1}^{n}\mathbb{E}^x\left[e^{-\alpha(\tau_\kappa - t)}\mathbb{1}_{\mathscr{E}_{\mathcal{J}}}\right]. \tag{86}$$

It will therefore suffice to compute either diffusion or jump contribution, since $\tilde{P}(x,\alpha) = \tilde{P}_D(x,\alpha) + \tilde{P}_J(x,\alpha)$, and the (total) price of a one-touch digital put optionette is given in Theorem 3. To compute, e.g., the diffusion contribution $\tilde{P}_D(x,\alpha)$, we have to solve the OIDE

$$\frac{\sigma^2}{2}\frac{d^2\tilde{P}_D}{dx^2}(x,\alpha) + \bar{\varrho}\frac{d\tilde{P}_D}{dx}(x,\alpha) - (\lambda+\alpha)\tilde{P}_D(x,\alpha) + \lambda\int_{-\infty}^{+\infty}\tilde{P}_D(x+y,\alpha)f_Y(y)dy = 0, \tag{87}$$

which is the same as the equation (72). The boundary conditions (73) remain unchanged as well. However, the diffusion contribution in the interior of the stopping region, i.e., for $x < \kappa$ is zero. This is a consequence of the fact that stopping due to diffusion can happen only at the boundary, i.e., almost surely a diffusion will not generate an overshoot. Therefore, we use the following ansatz:

$$\tilde{P}_D(S_t, \alpha) = \begin{cases} \sum_{j=1}^{\hat{n}} \delta_j \left(\frac{S_t}{K}\right)^{\gamma_{j,\alpha}} & \text{if } S_t > K, \\ 1 & \text{if } S_t = K, \\ 0 & \text{if } S_t \leq K. \end{cases} \tag{88}$$

Following the same procedure as in Appendix B.1 and Appendix B.2, we obtain the conditions that summations coefficients $\{\delta_j\}_{j=1,...,\hat{n}}$ have to satisfy:

$$\begin{cases} \sum_{j=1}^{\hat{n}} \frac{\delta_j e^{\gamma_{j,\alpha}\xi}}{\theta_l + \gamma_{j,\alpha}} = 0, \quad \text{for } l = 1, ..., n, \\ \sum_{j=1}^{\hat{n}} \delta_j = 1. \end{cases} \tag{89}$$

We rewrite these conditions in the matrix form

$$\mathbf{M}_D \boldsymbol{\delta} = \boldsymbol{\epsilon}_D, \tag{90}$$

where

$$\boldsymbol{\delta} := (\delta_1, \delta_2, ..., \delta_{\hat{n}})' \tag{91}$$

is $\hat{n}$-dimensional column vector, and

$$\boldsymbol{\epsilon}_D := \left(1, \underbrace{0, ..., 0}_{n \text{ times}}\right)' \tag{92}$$

is $(n+1)$-dimensional column vectors. The matrix $\mathbf{M}_D$ is $(n+1) \times \hat{n}$-dimensional matrix which is the same as the matrix $\mathbf{B}$, which is given in (83).

By analogy, it can be shown the summation coefficients $\{\iota_i\}_{j=1,...,\hat{m}}$ can be computed as the solution of the matrix equation

$$\mathbf{M}_J \boldsymbol{\iota} = \boldsymbol{\epsilon}_J, \tag{93}$$

where

$$\boldsymbol{\iota} := (\iota_1, \iota_2, ..., \iota_{\hat{m}})' \tag{94}$$

is $\hat{n}$-dimensional column vector, and

$$\boldsymbol{\epsilon}_J := \left(0, \frac{1}{\theta_1}, ..., \frac{1}{\theta_n}\right)' \tag{95}$$

is $(n+1)$-dimensional column vectors. The matrix $\mathbf{M}_J$ is $(n+1) \times \hat{n}$-dimensional matrix which is identical to the matrix $\mathbf{M}_D$.

This concludes the proof. ■

Appendix C Tables and Figures

Table 1: S&P 100 index options data, March, 2001–August, 2014. We report descriptive statistics for near-the-money (NTM) and out-of-the-money (OTM) S&P 100 American put options with maturities of up to 10 days. The data is obtained from OptionMetrics and filtered according to standard criteria. The dataset comprises closing quotes of liquid put options sampled on monthly frequency. The data treatment and the monthly time-stamping procedure are described in Section 4.1. There are 162 observation dates in total. We report the number of option contracts traded (Panel A), the average quoted price (Panel B) and the average implied volatility (Panel C). Each statistic is computed for three different maturity bins and four different moneyness bins, as well as for the entire sample, i.e., aggregated across the maturity and the moneyness dimension. DTM stands for days to maturity.

Panel A: Number of contracts across moneyness and maturity

Moneyness	DTM≤5	5<DTM≤9	DTM=10	All
K/F < 0.94	78	81	1,207	1,366
0.94<K/F<0.97	173	22	437	632
0.97<K/F<1.00	311	26	450	787
1.00<K/F<1.03	164	27	435	626
All	726	156	2,529	3,411

Panel B: Average quoted price across moneyness and maturity

Moneyness	DTM≤5	5<DTM≤9	DTM=10	All
K/F < 0.94	0.39	0.42	0.65	0.62
0.94<K/F<0.97	0.70	1.51	1.97	1.60
0.97<K/F<1.00	2.16	3.54	4.90	3.77
1.00<K/F<1.03	8.78	11.84	13.02	11.86
All	3.11	3.07	3.76	3.59

Panel C: Average implied volatility across moneyness and maturity

Moneyness	DTM≤5	5<DTM≤9	DTM=10	All
K/F < 0.94	0.4985	0.3721	0.3930	0.3978
0.94<K/F<0.97	0.3444	0.2467	0.2452	0.2724
0.97<K/F<1.00	0.2343	0.1960	0.2088	0.2184
1.00<K/F<1.03	0.2475	0.1988	0.1987	0.2115
All	0.2920	0.2951	0.3014	0.2991

Table 2: Summary statistics for parameter estimates. We estimate parameters of the Merton jump-diffusion (MJD), the finite-moment log-stable (FMLS), the variance gamma (VG), and the Carr-Geman-Madan-Yor (CGMY) model using the S&P 100 historical return time series data (Panel A) and the short-term S&P 100 American put options (Panel B). The total number of observations in our sample is 162 (monthly frequency). The table entries report the average values and the standard deviations (in parentheses) of the estimated parameters. Additionally, we include the values of the rolling-window negative log-likelihood based on the historical returns (MLE) and the weighted mean squared errors of the sequential option calibration (MSE). Detailed information about the data and the estimation techniques is provided in Section 4.1 and Section 4.2, respectively.

Panel A: Calibration under the historical measure					
Parameters	σ	λ	μ_J	σ_J	MLE
MJD	0.10	4.23	-0.32	0.14	4.62
	(0.03)	(5.56)	(0.49)	(0.18)	(0.18)
Parameters	C	G	M	Y	MLE
FMLS	0.0026	_	_	1.88	4.65
	(0.0017)			(0.07)	(0.17)
VG	549.78	184.40	110.48	_	4.63
	(5,102.29)	(408.29)	(289.99)		(0.17)
CGMY	14.22	3,033.41	2,145.64	1.24	4.68
	(77.36)	(876.54)	(1,003.31)	(0.27)	(0.18)
Panel B: Calibration under the risk-neutral measure					
Parameters	σ	λ	μ_J	σ_J	MSE
MJD	0.12	5.57	-0.05	0.07	3.11
	(0.09)	(13.86)	(0.06)	(0.04)	(3.48)
Parameters	C	G	M	Y	MSE
FMLS	0.0063	_	_	1.85	4.04
	(0.0097)			(0.08)	(4.00)
VG	18.83	1,711.59	66.00	_	3.50
	(32.29)	(7,982.77)	(374.41)		(3.53)
CGMY	254.39	716.62	14.92	0.95	2.90
	(991.68)	(1,526.60)	(22.43)	(0.95)	(3.45)

Table 3: Model performance (pairwise comparison). The table entries report the values of Vuong (1989)'s closeness test statistic for pairwise equivalence of non-nested models in terms of model performance. The statistics are computed for the pairwise combinations of the Merton jump-diffusion (MJD), the finite-moment log-stable (FMLS), the variance gamma (VG), and the Carr-Geman-Madan-Yor (CGMY) model. Panel A (Panel B) reports the pairwise statistics for the maximum likelihood estimation (weighted non-linear least squares estimation) under the historical (risk-neutral) measure. The null hypothesis is that there is no difference between the two models in terms of the closeness to the true data generating process, and the alternative is that one model is closer. Positive values of test statistic larger than 1.65 (2.32) imply, for the given pair of models, the domination of the first model over the second one at the confidence level of 95%(99%). Conversely, negative values of the test statistic smaller than -1.65 (-2.32) imply domination of the second model over the first model at the confidence level of 95%(99%)

Panel A: Pairwise model comparison under the historical measure				
Model	MJD	FMLS	VG	CGMY
MJD	—	-1.80	-2.91	11.87
FMLS	—	—	-1.65	17.77
VG	—	—	—	16.68
Panel B: Pairwise model comparison under the risk-neutral measure				
Model	MJD	FMLS	VG	CGMY
MJD	—	7.19	6.05	-5.26
FMLS	—	—	-3.61	-8.80
VG	—	—	—	-8.60

Table 4: VaR and iVaR multiples. The table reports average, median, and maximum multiples of the end-of-horizon value at risk (VaR) and the intra-horizon value at risk (iVaR)—computed for $\chi = 99.0\%$ and 99.9% confidence levels at 10-day monitoring horizon—for the Merton jump-diffusion (MJD), the finite-moment log-stable (FMLS), the variance gamma (VG), and the Carr-Geman-Madan-Yor (CGMY) model under the historical and the risk-adjusted measure. The analysis is based on the time series of S&P 100 historical returns and the short-term S&P 100 American put options over the period March, 2001–August, 2014. The models are re-estimated on monthly basis, hence generating the total number of 162 observation dates in the sample. For each considered model, the multiples are computed as ratios of the respective VaR and iVaR estimates and the benchmark VaR value, which is given as either 1% or 0.1% quantile of the normal distribution $\mathcal{N}(\hat{\mu}, \hat{\sigma}^2)$. More precisely, the benchmark VaR is equal to $(2.32\hat{\sigma} - \hat{\mu})$ and $(3.09\hat{\sigma} - \hat{\mu})$ for the 99.0% and 99.9% confidence level, respectively. The parameter $\hat{\sigma}$ is the standard deviation of the (demeaned) time series of S&P 100 historical returns used for the estimation under the historical measure on a given day. The location parameter $\hat{\mu}$ is set to zero. We also report (in parentheses) the VaR and the iVaR multiples of our jump models w.r.t. the VaR estimates based on the filtered historical simulation (FHS) approach.

Panel A: Historical VaR & iVaR multiples

χ= **99.0**%	MJD	FMLS	VG	CGMY
Avg. VaR	1.11 (0.73)	1.20 (0.79)	1.20 (0.79)	1.00 (0.66)
Med. VaR	1.11 (0.73)	1.19 (0.76)	1.21 (0.77)	0.99 (0.65)
Max. VaR	1.99 (1.24)	1.70 (1.13)	1.85 (1.15)	1.26 (0.87)
Avg. iVaR	1.19 (0.79)	1.29 (0.85)	1.29 (0.85)	1.07 (0.71)
Med. iVaR	1.21 (0.78)	1.28 (0.82)	1.30 (0.83)	1.06 (0.70)
Max. iVaR	2.16 (1.35)	1.83 (1.22)	1.99 (1.24)	1.35 (0.93)
χ= **99.9**%	MJD	FMLS	VG	CGMY
Avg. VaR	1.38 (0.85)	1.99 (1.23)	1.32 (0.81)	1.00 (0.62)
Med. VaR	1.39 (0.81)	2.03 (1.20)	1.34 (0.80)	0.98 (0.61)
Max. VaR	2.47 (1.63)	3.43 (2.11)	2.09 (1.20)	2.65 (1.02)
Avg. iVaR	1.43 (0.88)	2.07 (1.28)	1.37 (0.85)	1.04 (0.65)
Med. iVaR	1.43 (0.84)	2.11 (1.25)	1.39 (0.83)	1.02 (0.64)
Max. iVaR	2.59 (1.71)	3.52 (2.17)	2.19 (1.25)	1.73 (1.08)

Panel B: Risk-adjusted VaR & iVaR multiples

χ= **99.0**%	MJD	FMLS	VG	CGMY
Avg. VaR	1.61 (1.06)	1.69 (1.11)	1.87 (1.23)	1.81 (1.19)
Med. VaR	1.37 (1.94)	1.35 (0.89)	1.51 (1.01)	1.49 (0.99)
Max. VaR	6.57 (3.93)	7.52 (4.50)	7.41 (4.43)	7.61 (4.55)
Avg. iVaR	1.69 (1.11)	1.83 (1.20)	2.02 (1.32)	1.95 (1.28)
Med. iVaR	1.42 (0.96)	1.46 (0.96)	1.65 (1.08)	1.61 (1.07)
Max. iVaR	6.82 (4.07)	8.04 (4.81)	7.90 (4.72)	8.12 (4.86)
χ= **99.9**%	MJD	FMLS	VG	CGMY
Avg. VaR	2.28 (1.40)	2.87 (1.77)	2.15 (1.31)	2.47 (1.51)
Med. VaR	2.15 (1.33)	2.58 (1.57)	1.82 (1.15)	2.27 (1.38)
Max. VaR	7.15 (3.28)	8.11 (4.19)	7.36 (3.38)	9.96 (5.63)
Avg. iVaR	2.35 (1.44)	2.99 (1.84)	2.25 (1.38)	2.57 (1.57)
Med. iVaR	2.22 (1.35)	2.69 (1.65)	1.92 (1.21)	2.36 (1.43)
Max. iVaR	7.29 (3.35)	8.48 (4.20)	7.62 (3.50)	9.96 (5.63)

Table 5: VaR and iVaR backtesting. The table summarizes the backtesting results for the end-of-horizon value at risk (VaR) and the intra-horizon value at risk (iVaR)—computed at the confidence level of $\chi = 99.0\%$, and for the regulatory 10-day monitoring period—for the Merton jump-diffusion (MJD), the finite-moment log-stable (FMLS), the variance gamma (VG), and the Carr-Geman-Madan-Yor (CGMY) model under the historical and the risk-adjusted measure. Additionally, we provide test statistics for the filtered historical simulation (FHS). The table reports the likelihood ration (LR) and the p-value (p-val.) for the following backtesting procedures: the Time Until First Failure test (TUFF), the Unconditional Coverage test (UC), the Independence Coverage test (IC), and the Conditional Coverage test (CC). Based on the test statistics, the historical (the risk-adjusted) approach to the estimation of VaR and iVaR is mostly rejected (mostly cannot be rejected) at the conventional confidence levels of 95% and 99%.

Panel A: Historical VaR backtesting

Method	#	TUFF		UC		IC		CC	
		LR	p-val.	LR	p-val.	LR	p-val.	LR	p-val.
FHS	6	1.9225	0.1652	6.9629	0.0083	6.5053	0.0108	13.4682	0.0012
MJD	7	9.2103	0.0024	9.7092	0.0018	5.8424	0.0156	15.5525	0.0004
FMLS	6	1.9225	0.1652	6.9629	0.0083	6.5053	0.0108	13.4682	0.0012
VG	7	9.2103	0.0024	9.7762	0.0018	5.8195	0.0158	15.5957	0.0004
CGMY	7	9.2103	0.0024	9.7762	0.0018	5.8195	0.0158	15.5957	0.0004

Panel B: Risk-adjusted VaR backtesting

Method	#	TUFF		UC		IC		CC	
		LR	p-val.	LR	p-val.	LR	p-val.	LR	p-val.
MJD	1	1.9225	0.1652	0.3010	0.5832	0.0123	0.9951	0.3133	0.8550
FMLS	0	0.2931	0.5882	3.2965	0.0694	0.0000	1.0000	3.2965	0.1925
VG	0	0.2931	0.5882	3.2965	0.0694	0.0000	1.0000	3.2965	0.1925
CGMY	1	0.1863	0.6660	0.2931	0.5882	0.0123	0.9619	0.3055	0.8584

Panel C: Historical iVaR backtesting

Method	#	TUFF		UC		IC		CC	
		LR	p-val.	LR	p-val.	LR	p-val.	LR	p-val.
FHS	8	3.5893	0.0582	12.8887	0.0003	9.0679	0.0026	21.9566	$<10^{-4}$
MJD	11	9.2103	0.0024	23.5822	$<10^{-4}$	10.2772	0.0013	33.8594	$<10^{-4}$
FMLS	8	3.5893	0.0582	12.8887	0.0003	9.0679	0.0026	21.9566	$<10^{-4}$
VG	9	3.5893	0.0582	16.2644	0.0001	7.4684	0.0063	23.7338	$<10^{-4}$
CGMY	9	3.5893	0.0582	16.2644	0.0001	7.4684	0.0063	23.7338	$<10^{-4}$

Panel D: Risk-adjusted iVaR backtesting

Method	#	TUFF		UC		IC		CC	
		LR	p-val.	LR	p-val.	LR	p-val.	LR	p-val.
MJD	1	0.1426	0.7057	0.3010	0.5832	0.0123	0.9118	0.3133	0.8550
FMLS	0	0.2931	0.5882	3.2965	0.0694	0.0000	1.0000	3.2965	0.1924
VG	0	0.2931	0.5882	3.2965	0.0694	0.0000	1.0000	3.2965	0.1924
CGMY	1	0.1863	0.6660	0.2931	0.5882	0.0123	0.9115	0.3055	0.8584

Figure 1: D-MEM examples. Two examples of displaced-mixed exponential models (D-MEM) are presented to illustrate the equations (1) and (5)–(6). We arbitrarily set the drift of the asset price process to $\mu = 0.02$. Both models have three types of ξ^+ and ξ^--jumps, and we assume the following parameter values. The displacement parameter is $\xi = -0.05$. The positive and the negative jump intensites are equal and set to $\lambda_+ = \lambda_- = 5$. The volatility parameter is $\sigma = 0.2$. The ξ^+-jump size parameters are $\eta = (20, 50, 100)$, and the ξ^--jump size parameters are $\theta = (5, 20, 50)$. However, the conditional probabilities of the occurence of different jump types are not the same for the two models. In the first model, ξ^+-jumps have probabilities $p = (0.1, 0.2, 0.7)$ and ξ^--jumps have probabilities $q = (0.2, 0.3, 0.5)$. Because all mixing weights are positive, this is a displaced *hyper*-exponential model, here denoted by D-HEM(3,3). In the second model, the ξ^+-jumps have probabilities $p = (0.4, -0.2, 0.8)$ and the ξ^--jumps have probabilities $q = (0.5, -0.5, 1.0)$. In this case, some of the mixing weights are negative, hence this is a displaced *mixed*-exponential model and we denote it by D-MEM(3,3). Panels A and B represent the p.d.f. and the characteristic exponent of the D-HEM(3,3) model, respectively. Similarly, Panels C and D represent respective plots of the p.d.f. and the characteristic exponent of the D-MEM(3,3) model. Shaded area in the Panel D is the subspace of the positive y-semiaxis where characteristic equation $\Psi(u) = \alpha$ (for $\alpha \in \mathbb{R}^+$) does not have $n + m + 2 = 8$ distinct real roots. In fact, this is satisfied only for sufficiently large parameter α; see Theorem 3.1 in Cai and Kou (2011), pp. 2071–2072. On the other hand, Panel C does not display such a feature because any D-HEM(n, m) model (for $n, m \in \mathbb{N}$) has exactly $(n + m + 2)$ distinct real roots if $\sigma > 0$; this statement can be proved by generalizing Lemma 2.1. in Cai (2009), pp. 128–129.

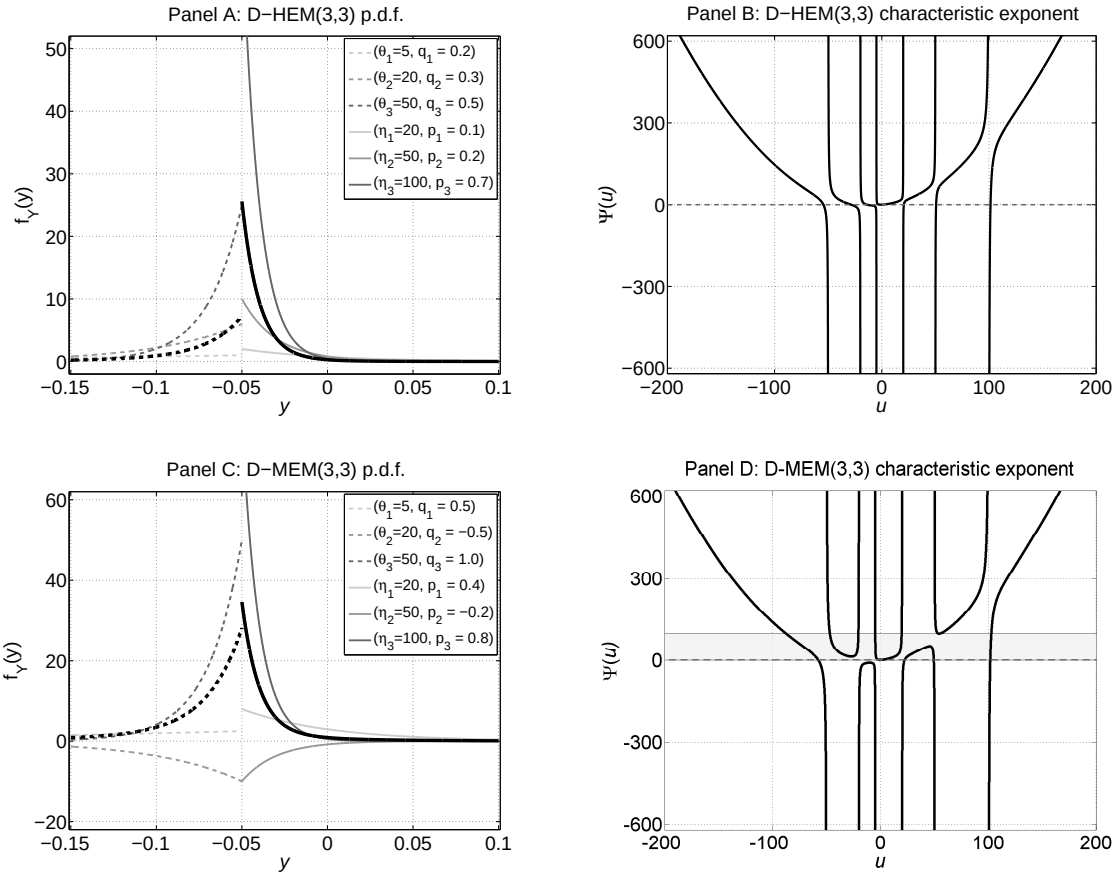

Figure 2: Volatility and expected jumps size (D-MEM approximation). The plots represent the time evolution (monthly frequency) of biweekly (diffusion) volatility $\sigma_b := \sigma\sqrt{\tau}$ and the expected jump size $\iota_b := \lambda\zeta\tau$ of log-price process over the time horizon of 10 days, i.e., $\tau = 10/252$. The parameter λ is the jump intensity, and the parameter ζ is defined in (4). The model parameters are estimated by approximating the Merton jump-diffusion (MJD), the finite-moment log-stable (FMLS), the variance gamma (VG), and the Carr-Geman-Madan-Yor (CGMY) model with displaced mixed-exponential models (D-MEM) under the historical and the risk-adjusted measure. Panels A and C (B and D) represent the evolution of the volatility (the expected jump sizes) for the considered models under the historical and the risk-adjusted measure, respectively.

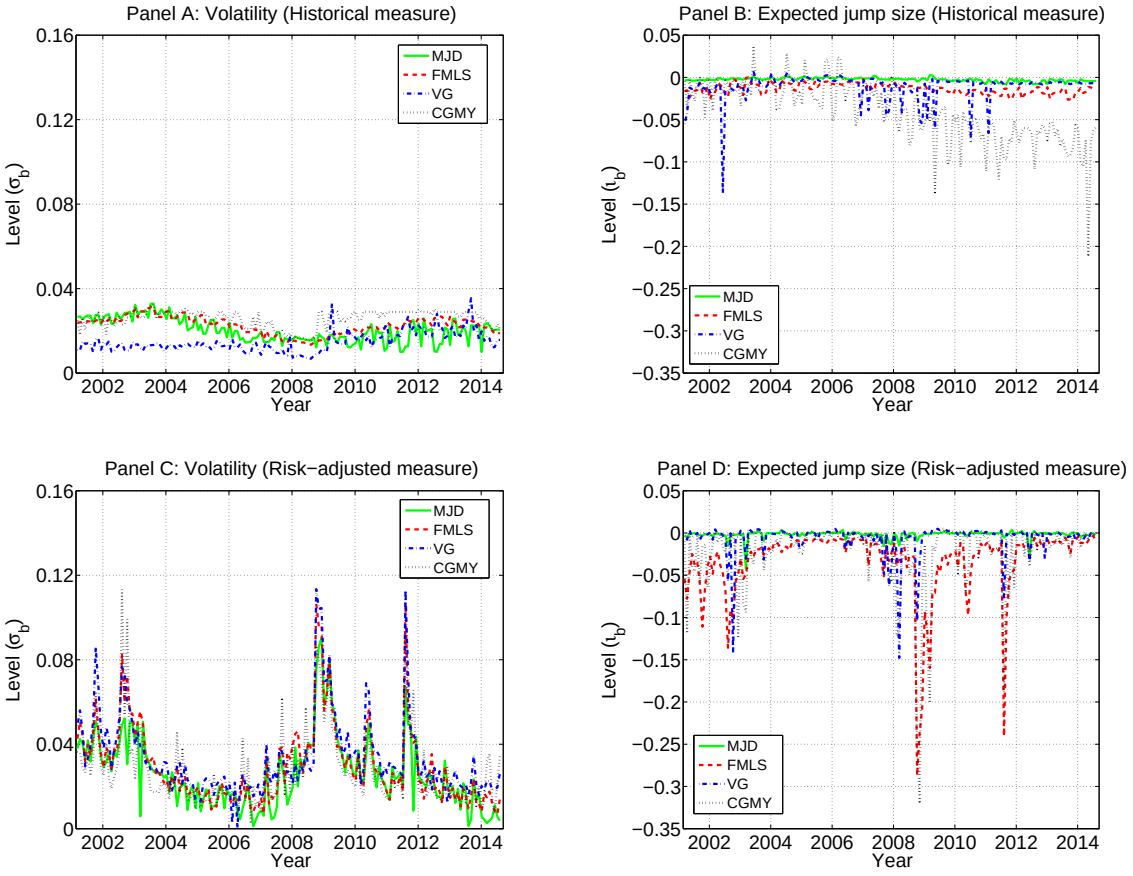

Figure 3: First-passage disentanglement of the iVaR (10-day horizon, 99.0% confidence level). For each considered model—the Merton jump-diffusion (MJD), the finite-moment log-stable (FMLS), the variance gamma (VG), and the Carr-Geman-Madan-Yor (CGMY) model, which are given in Panels A, B, C, and D, respectively—we plot the time evolution of the jump contribution to the 10-day intra-horizon value at risk (iVaR) calculated at the confidence level of 99.0%. Our results are based on the first-passage disentanglement (FPD) approach introduced in Section 3.3. For each of the four models, the jumps are contributing by approximately 90% to the iVaR. These findings hold under the historical and the risk-adjusted measure alike. Interestingly, the model and the estimation risk seem to have significantly smaller impact on the FPD results relative to the backtesting results presented in Figure 6 and Figure 7.

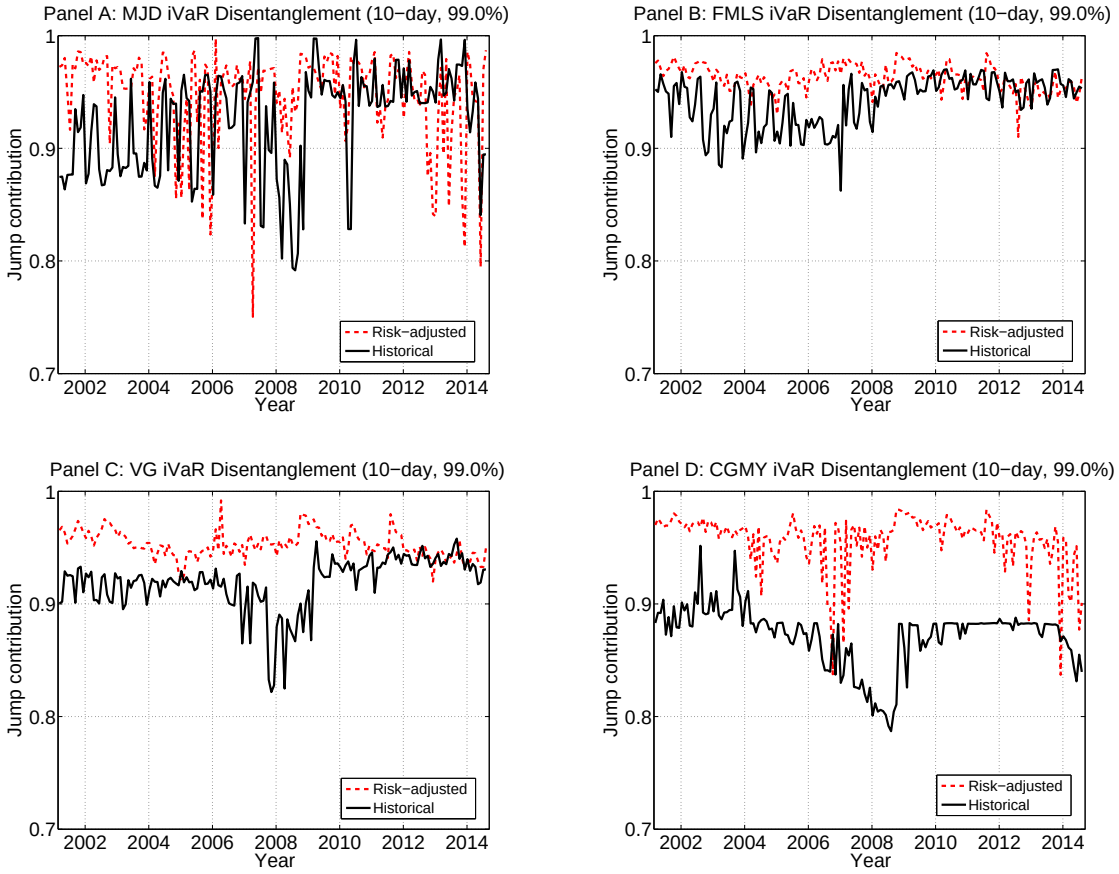

Figure 4: iVaR multiples across models (10-day horizon, 99.0% confidence level). For each considered model—the Merton jump-diffusion (MJD), the finite-moment log-stable (FMLS), the variance gamma (VG), and the Carr-Geman-Madan-Yor (CGMY) model, which are given in Panels A, B, C, and D, respectively—we plot the time evolution of the ratio of the intra-horizon value at risk (iVaR) to the end-of-horizon value at risk (VaR), estimated under the historical and the risk-adjusted measure at the confidence level of 99.0% and with the monitoring horizon of 10 days.

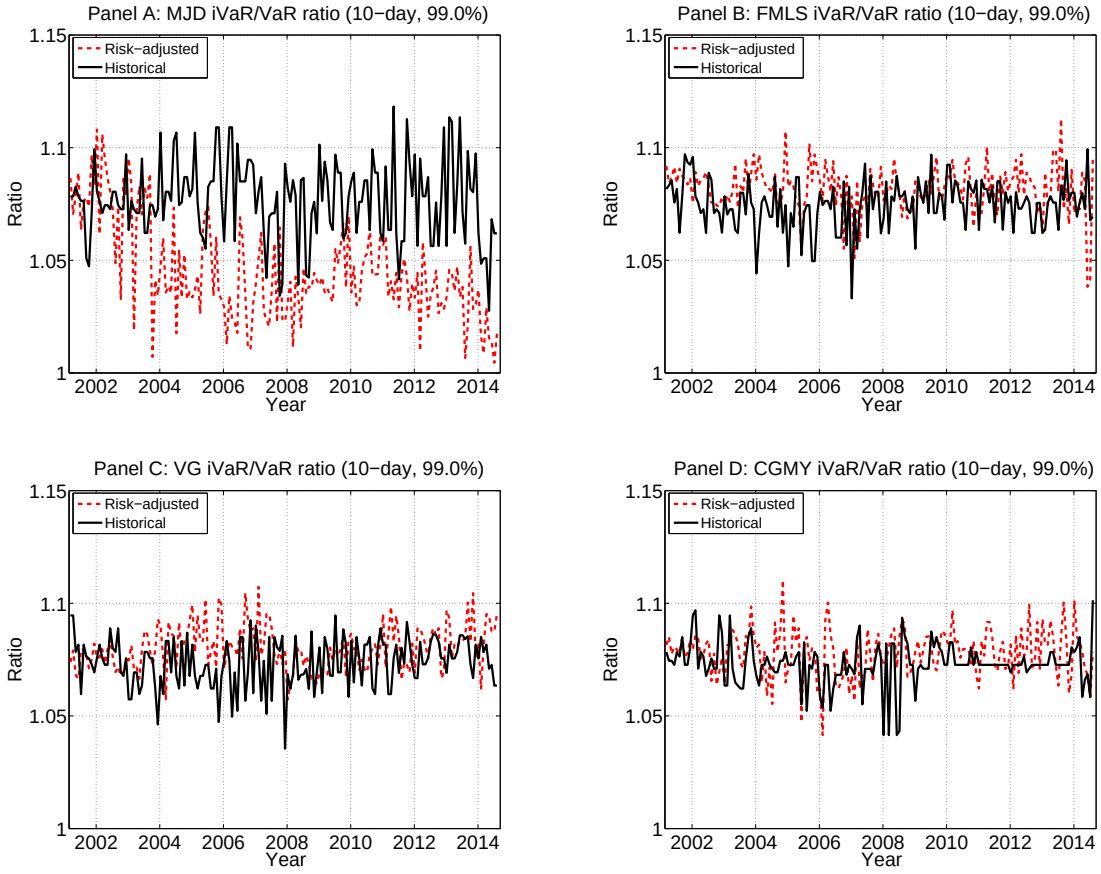

Figure 5: The impact of the probability measure on iVaR (10-day horizon, 99.0% confidence level). For each considered model—the Merton jump-diffusion (MJD), the finite-moment log-stable (FMLS), the variance gamma (VG), and the Carr-Geman-Madan-Yor (CGMY) model—we plot the time evolution of the ratio of the risk-adjusted to historical intra-horizon value at risk (iVaR) calculated at the confidence level of 99.0%, and with monitoring horizon of 10 days.

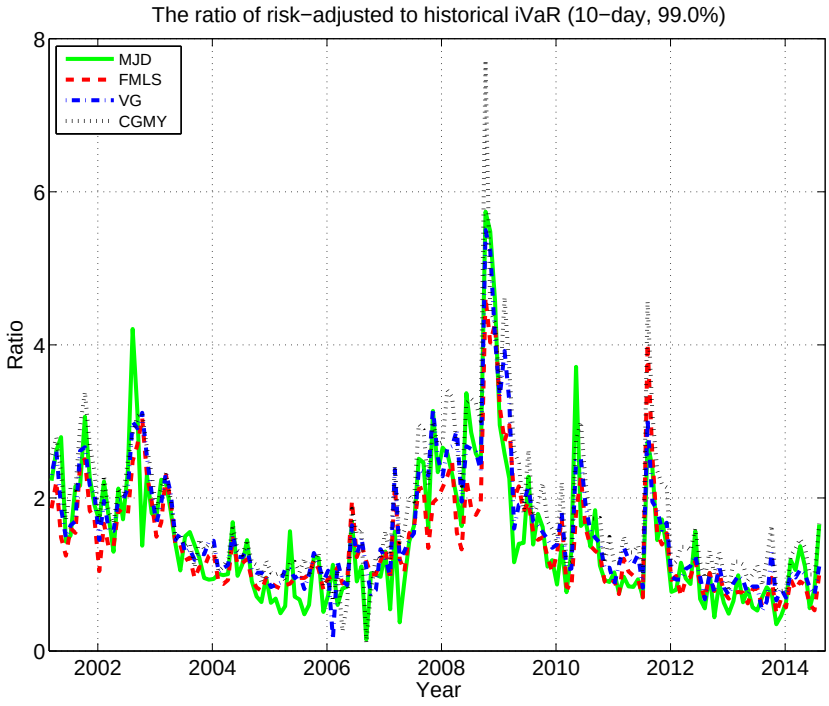

Figure 6: VaR backtesting (10-day horizon, 99.0% confidence level). For each considered model—the Merton jump-diffusion (MJD), the finite-moment log-stable (FMLS), the variance gamma (VG), and the Carr-Geman-Madan-Yor (CGMY) model, which are given in Panels A, B, C, and D, respectively—we graphically represent the time evolution of the 10-day end-of-horizon value at risk (VaR) calculated at the confidence level of 99.0% and the realized 10-day returns. We plot the estimates under both the historical and the risk-adjusted measure. Additionally, we include the VaR estimates based on a filtered historical simulation (FHS). The plots provide information about the ability of each model to forecast the VaR of the S&P 100 index *at the end* of the regulatory 10-day horizon. Although the model risk seems to be important, the results are particularly sensitive to the estimation risk, i.e., the risk-adjusted estimates better forecast market moves than the historical estimates.

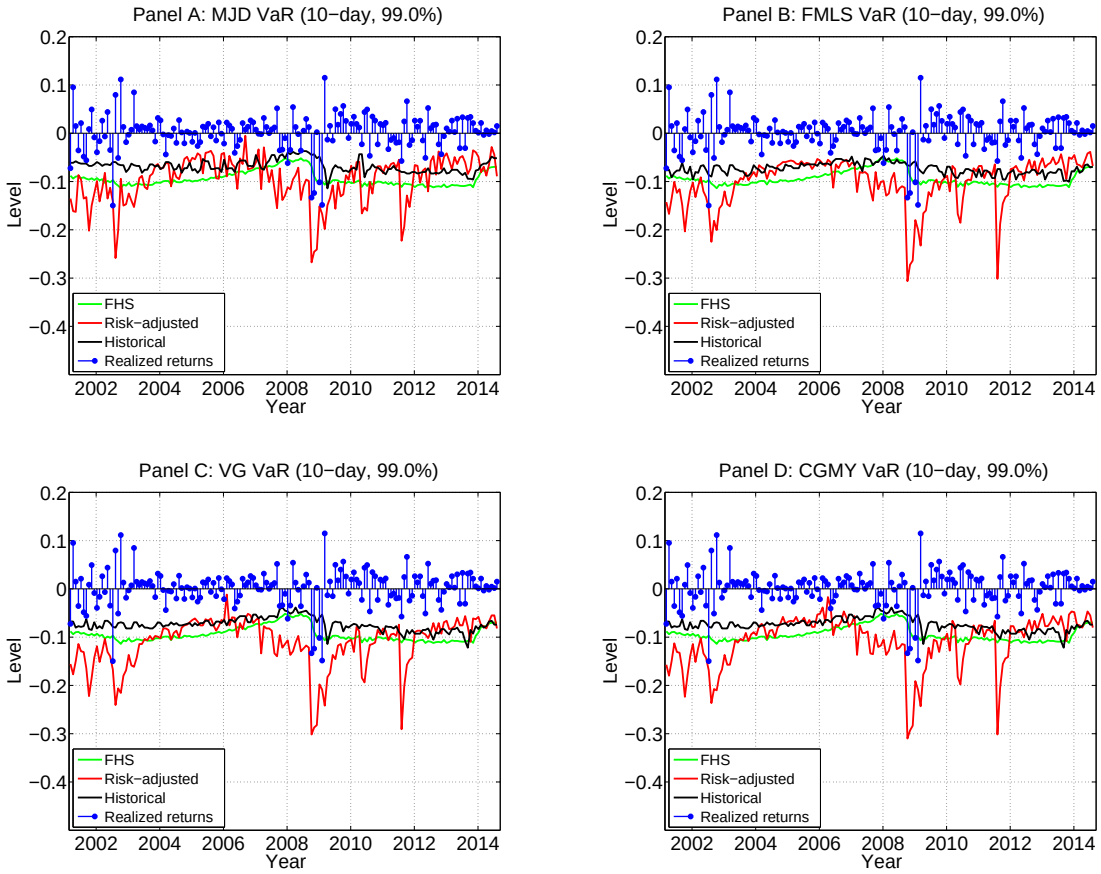

Figure 7: iVaR backtesting (10-day horizon, 99.0% confidence level). For each considered model—the Merton jump-diffusion (MJD), the finite-moment log-stable (FMLS), the variance gamma (VG), and the Carr-Geman-Madan-Yor (CGMY) model, which are given in Panels A, B, C, and D, respectively—we graphically represent the time evolution of the 10-day intra-horizon value at risk (iVaR) calculated at the confidence level of 99.0% and the realized minimal cumulative interim 10-day returns. We plot the estimates under the historical and the risk-adjusted measure. Additionally, we include the iVaR estimates based on a filtered historical simulation (FHS). The plots provide information about the ability of each model to forecast the iVaR of the S&P 100 index *within* the regulatory 10-day horizon. Similarly to the VaR case, we conclude that model risk matters also for the iVaR, but the results are again markedly more sensitive to the estimation risk.